

1 **Refined burned-area mapping protocol using Sentinel-2 data**  
2 **increases estimate of 2019 Indonesian burning**

3 David L.A. Gaveau<sup>1</sup> Adria Descals<sup>2</sup>, Mohammad A. Salim<sup>1</sup>, Douglas Sheil<sup>3</sup>, Sean Sloan<sup>4,5</sup>

4 <sup>1</sup> TheTreeMap Bagadou Bas 46600 Martel, France

5 <sup>2</sup> CREAM, Centre de Recerca Ecològica i Aplicacions Forestals, E08193 Bellaterra (Cerdanyola de Vallès),  
6 Catalonia, Spain

7 <sup>3</sup> Forest Ecology and Forest Management Group, Wageningen University & Research, PO Box 47, 6700 AA,  
8 Wageningen, The Netherlands

9 <sup>4</sup> Department of Geography, Vancouver Island University, Nanaimo, BC, Canada &

10 ~~<sup>5</sup>Fenner School of Environment and Society, Australia National University, Canberra, ACT, Australia~~

11 Correspondence to: David Gaveau (d.gaveau@thetreemap.com)

12

## 14 Abstract

15 ~~Like many tropical forest~~Many nations, ~~Indonesia is~~ are challenged by landscape fires. ~~Given the significant~~  
 16 ~~impacts that burning episodes have on the global carbon cycle and on human health across South East Asia. A a~~  
 17 confident ~~understanding knowledge~~ of the area and distribution of burning is crucial to ~~understanding quantify~~  
 18 ~~monitor the implications impacts~~ of these fires and ~~to assess~~ how they might best be reduced. Given ~~uncertainties~~  
 19 ~~surrounding different burned area estimates, and~~ the ~~substantial~~ differences that arise using different ~~detection~~  
 20 approaches, ~~and the uncertainties and debates that surrounding such results~~burned-area estimates, their relative~~the~~  
 21 ~~accuracy, and merits of such estimates~~ require ~~formal examination~~evaluation. ~~Here we propose, illustrate, and~~  
 22 ~~examine one promising approach for Indonesia.~~

23 ~~Despite investment in fire mitigation measures since the severe El Niño 2015 fire season, severe burning struck~~  
 24 ~~Indonesia again in late 2019. D~~Here, drawing on Sentinel-2 satellite time-series analysis, we present and validate  
 25 new 2019 burned-area estimates for Indonesia. The corresponding burned-area map is available at:  
 26 ~~https://doi.org/10.5281/zenodo.4551243.~~ We show that >3.11 million hectares (Mha) burned in 2019, ~~31% of~~  
 27 ~~which on peatlands.~~ This burned-area extent is double the Landsat-derived Official estimate of 1.64 Mha from the  
 28 Indonesian Ministry of Environment and Forestry, and 50% more than the MODIS MCD64A1 burned-area  
 29 estimate of 2.03 Mha. ~~Though we observed proportionally less peatland burning (31% versus 39% and 40% for~~  
 30 ~~the Official and MCD64A1 products, respectively), in absolute terms we still observed more peatland burning~~  
 31 ~~absolutely~~a greater area of peatland affected (0.96 Mha) than the official estimate (0.64 Mha). - ~~This new burned-~~  
 32 ~~area dataset~~ has greater reliability as these alternatives, attaining a user's accuracy of 97.9% (CI: 97.1%-98.8%)  
 33 compared to 95.1% (CI: 93.5%-96.7%) and 76% (CI: 73.3%-78.7%), respectively. It omits fewer burned areas,  
 34 particularly smaller- (<100 ha) to intermediate-sized (~~100 ha~~ -1000 ha) burns~~sears~~, attaining a producer's  
 35 accuracy of 75.6% (CI: 68.3%-83.0%) compared to 49.5% (CI: 42.5%-56.6%) and 53.1% (CI: 45.8%-60.5%),  
 36 respectively. The frequency-area distribution of the Sentinel-2 burns~~sears~~ follows the apparent fractal-like power-  
 37 law or "pareto" pattern often reported in other ~~extensive~~ fire studies, suggesting good detection over several  
 38 magnitudes of scale. Our relatively accurate estimates have important implications for carbon-emission  
 39 calculations from forest and peatland fires in Indonesia. ~~Our approach is amenable to the ongoing production of~~  
 40 ~~accurate annual burned area maps for environmental monitoring and policy in South East Asia.~~

41

## 42 1. Introduction

43 ~~The accurate identification and characterization of landscape fires supports interventions to reduce their severity~~  
 44 ~~and impacts. Refined~~Accurate burned area maps are key to ~~characterizing refine C emissions from~~ landscape fires,  
 45 ~~clarifying emissions and to~~identifying the probable causes. Such information is needed to target interventions, to  
 46 ~~identify the result of~~assess policies and practices intended to reduce or control fires, such as law enforcement and  
 47 ~~restoration of fire-prone degraded lands, and to measure progress to international climate commitments (Sloan et~~  
 48 ~~al., 2021). Such support is needed in extensive tropical regions where fires are a major concern (REF). Here, we~~  
 49 ~~focus on Landscape f~~Forest and peatland fires in Indonesia where recurring ~~landscape~~forest and peatland fires;  
 50 ~~and their consequences, are~~have become an cause of major international ~~concern~~crisis (Tacconi, 2016)(REF).  
 51 ~~These concerns arise from the major~~large carbon ~~because of the large GHG~~ emissions associated with these

52 fires, and the ~~negative~~ impact of associated aerosol emissions for human health in the ~~Southeast Asian~~ wider  
53 ~~region~~ are a global concern due to their impacts (Van der Werf et al., 2008; Marlier et al., 2013) (~~REF~~).  
54 Although fires have occurred locally in Southeast Asia for millennia, they are increasingly frequent in Indonesia's  
55 disturbed forests and deforested peatlands (Field et al., 2009; Gaveau et al., 2014). The causes and motivations of  
56 fire use can be complex (Dennis et al., 2005), but many fires are lit to create or maintain agricultural land (Gaveau  
57 et al., 2014; Adrianto et al., 2020). ~~While human activities are the main cause of ignition local conditions govern~~  
58 ~~the likelihood of burns spreading.~~ Most ~~burns~~ fires occur during drier months ~~and years~~ (July to October) and the  
59 threats are greatly heightened during ~~periods~~ years of anomalously low rainfall (Sloan et al., 2017; Field et al.,  
60 2016). During 2015, a strong El Niño-induced drought year, fires burned an estimated 2.6 million hectares  
61 according to official estimates (Sipongi, 2020). Although 2015 burning was approximately half as extensive as  
62 1997, the most severe El Niño and fire season on record (Fanin and Werf, 2017), about 50% more peatlands  
63 burned (Fanin and Werf, 2017). The 2015 fires emitted between 0.89 and 1.5 billion tons of CO<sub>2</sub>  
64 equivalent (Huijnen et al., 2016; Lohberger et al., 2018; Van Der Werf et al., 2017), representing about half of  
65 Indonesia's ~~total~~ greenhouse gas emissions for that year (Gütschow et al., 2019). In Palangkaraya, the capital city  
66 of Central Kalimantan province, daily average particulate matter (PM<sub>10</sub>) concentrations often reached 1000 to  
67 3000 µg m<sup>-3</sup> amongst the worst sustained air quality ever recorded worldwide (Wooster et al., 2018). Over half a  
68 million people suffered respiratory problems in the aftermath, and between 12,000 and 100,000 premature deaths  
69 were estimated (Kopplitz et al., 2016; Crippa et al., 2016). ~~Other~~ These impacts include wildlife  
70 ~~habitat~~ ecosystems loss and degradation of habitats with high conservation values, ~~the associated emissions of~~  
71 ~~greenhouse gases and toxic smoke,~~ and the associated consequences for impacted wildlife (Harrison et al., 2016).  
72  
73 (~~REF~~), human health, transport, tourism, and economic activity across Southeast Asia. Fires, though scarce in wet  
74 forest landscapes, have long been an element of traditional ~~swidden~~ agriculture and land clearance. Although the  
75 causes and motivations of modern-day fire use can be complex (Dennis et al., 2005), many fires are lit by farmers  
76 and ~~plantation~~ companies when conditions permit to burn wood debris ~~after deforestation,~~ and enrich the soils  
77 before planting, or to maintain existing agricultural land (paddy farm fallow) (Gaveau et al., 2014; Adrianto et al.,  
78 2020) or to maintain existing agricultural land (paddy fields, farm fallow). ~~Burning occurs throughout the year,~~  
79 ~~but generally more often during dry months from July to October.~~ The likelihood, scale and intensity of such fires  
80 are greatly heightened during periods of anomalously low rainfall (Sloan et al., 2017; Field et al., 2016). ~~Droughts~~  
81 ~~are associated with years when anomalously cold sea surface temperatures surround Indonesia and warm waters~~  
82 ~~develop in the eastern Pacific Ocean (El Niño Southern Oscillation, ENSO) and in the western Indian Ocean~~  
83 ~~(Positive Indian Ocean Dipole, IOD+) (Field et al., 2009), although short, but intense, fire episodes can occur~~  
84 ~~during climatically normal years, or under Julian Madden weather conditions (Gaveau et al., 2014; Kopplitz et al.,~~  
85 ~~2018).~~ ~~as~~ During drought years, fires readily spread uncontrolled beyond the intended areas (Gaveau et al., 2017),  
86 largely over degraded lands (Miettinen et al., 2017; Lohberger et al., 2018) but ~~can~~ also penetrate into ~~logged over~~  
87 ~~and intact forests~~ near the edge (Nikonovas et al., 2020). Intact rainforests don't burn without the prolonged  
88 droughts that favor the accumulation of sufficient dry fuel, and while many live trees often remain (van Nieuwstadt  
89 and Sheil, 2005) the resulting changes to forest structure increase the likelihood of further fires (Nikonovas et al.,  
90 2020; Cochrane, 2003). In Indonesia, droughts are often associated with years when anomalously cold sea surface  
91 temperatures surround Indonesia and warm waters develop in the eastern Pacific Ocean (El Niño Southern  
92 Oscillation, ENSO) and in the western Indian Ocean (Positive Indian Ocean Dipole, IOD+) (Field et al., 2009),  
93 although short, but intense, fire episodes can also occur during climatically normal years, or under Julian Madden

94 weather conditions (Gaveau et al., 2014; Koplitz et al., 2018). Austin et al. (2019) estimated that forest conversion  
95 to grasslands by repeated fires accounted for 20% of total forest loss in Indonesia between 2001 and 2016.  
96 The location, context, extent, and timing of fires have major implications for their impacts and their management.  
97 Many fires are started intentionally as a traditional, and low cost way to clear land. During drought years in  
98 particular they often spread beyond the intended areas (Gaveau et al., 2017), largely over degraded lands  
99 (Miettinen et al., 2017; Lohberger et al., 2018) but can also penetrate into logged over and intact forests  
100 (Nikonovas et al., 2020). Intact rainforests don't burn without the prolonged droughts that favor the accumulation  
101 of sufficient dry fuel, and while many live trees often remain (van Nieuwstadt and Sheil, 2005) the resulting  
102 changes to forest structure increase the likelihood of further fires (Nikonovas et al., 2020; Cochrane, 2003). Careful  
103 observation of burns can help identify the source and origins of the fires (e.g. Gaveau et al 2014). During 2015,  
104 a strong El Niño year, fires burned an estimated 2.6-4.5 million hectares across Indonesia (Sipongi,  
105 2020; Lohberger et al., 2018) and emitted 1.2 billion tons of CO<sub>2</sub>-equivalent (or 884 million tons of CO<sub>2</sub>) (Huijnen  
106 et al., 2016), representing half of Indonesia's total greenhouse gas emissions for that year (Gütschow et al., 2019).  
107 In Palangkaraya, the capital city of Central Kalimantan province, daily average particulate matter (PM<sub>10</sub>)  
108 concentrations often reached 1000 to 3000 µg m<sup>-3</sup> amongst the worst sustained air quality ever recorded worldwide  
109 (Wooster et al., 2018). For reference, 50 µg m<sup>-3</sup> is a short-term (24-h) exposure limit set by the World Health  
110 Organization (WHO), and 300 µg m<sup>-3</sup> is "extremely hazardous" according to by the Singapore National  
111 Environment Agency. Over half a million people suffered respiratory problems in the aftermath, and between  
112 12,000 and 100,000 premature deaths were estimated to result (Koplitz et al., 2016; Crippa et al., 2016). Although  
113 2015 burning was approximately half as severe/extensive as 1997, the most severe El Niño and fire season on  
114 record (Fanin and Werf, 2017), about 50% more peatlands burned about 50% more extensively in 2015 (Fanin  
115 and Werf, 2017). This pattern tracks a growing incidence of elevated peatland burning despite apparent long-  
116 term mitigation (declines) to extreme fire activity (Sloan et al., Under Review).

117 In response to the catastrophic 2015 fires, the Indonesian government instituted several ambitious schemes  
118 including fire bans enforced by dedicated command posts (Sloan et al., Under Review 2021) and an ambitious  
119 national program of peatland restoration (Carmenta et al., 2020).

120 In response to severe 2015 burning, the Indonesian government instituted several ambitious mitigation schemes.  
121 Fire bans were enforced by dedicated command posts established in 731 fire prone agricultural villages or *desas*  
122 (~12 Mha), recently expanded to some 4000 village areas, with some apparent success in suppressing burning  
123 (Sloan et al., Under Review). Simultaneously, in recognition that degraded peatlands are the primary source of  
124 haze, the government pursued a new peatland restoration agenda. The Peatland Restoration Agency or *Badan*  
125 *Restorasi Gambut* (BRG) was established in 2016 and declared a 2.67 Mha peatland restoration target across 7  
126 provinces host to >70% of the national burned area (Kalimantan Barat, Kalimantan Tengah and Kalimantan  
127 Selatan, Papua, Jambi, Riau, and Sumatra Selatan). The seven provinces are largely the same as those actively  
128 enforcing targeted fire bans. Restoration and fire suppression initiatives driven by pulp and paper and agro-  
129 industrial companies severely impacted by fire also flourished (Carmenta et al., 2020). These companies are  
130 mandated to actively restore some of the targeted for restoration degraded peatlands (2.67 Mha).

131  
132 Despite the investment in these approaches and measures since 2015, and some initial success, severe burning  
133 struck Indonesia again in late 2019. This time a positive Indian Ocean Dipole event, rather than an ENSO weather  
134 system, was responsible for widespread droughts, although the changing nature of these relationships and other  
135 weather phenomenon remain a subject of ongoing research (Kurniadi et al., 2021; Cai et al., 2021). While Sloan

136 et al. (~~Under Review~~2021) suggest that 2019 fire activity was lower than ~~might have occurred under the conditions~~  
137 ~~otherwise expected given the severe drought conditions~~, the total number of MODIS active-fire detections in late  
138 2019 ~~on peatlands~~ was still amongst the greatest recorded since 2001 ~~in the village areas targeted for fire~~  
139 ~~suppression, excepting 2015~~-(Sloan et al., ~~2021~~Under Review). However, ~~counts of active fire detections are not~~  
140 ~~the same as~~ counts of active-fire detections ~~are not the same as~~ don't provide estimates of area burned (Tansey et  
141 al., 2008) and for 2019 such ~~area~~ estimates remain uncertain. ~~estimates of area burned (Tansey et al., 2008) and for~~  
142 ~~2019 such area estimates remain uncertain. (REF).~~

143  
144 ~~Those wishing to assess and monitor burned areas have various approaches to consider. and to identify the sources~~  
145 ~~and probably causes Such information is needed to target interventions, to~~ and international

146  
147 ~~Accurate estimates of burned lands, and in particular assessments of peat fires, are key to ambitious Indonesian~~  
148 ~~climate change atmospheric carbon (C) reduction national commitments (DGCC, 2019). Burned area estimates~~  
149 ~~are used to calculate annual C emissions from fires, contribute to forensic analyses in landholdings (e.g. oil palm~~  
150 ~~and pulp & paper concessions), and help identify the result of policies and practices intended to reduce or control~~  
151 ~~fires, such as land enforcement and restoration of degraded lands.~~

152  
153 ~~Several global burned area products generated using coarse-resolution satellites (>250 m) can be applied over~~  
154 ~~Indonesia. These include the FireCCI41 product derived from Envisat-MERIS (Alonso-Canas and Chuvieco,~~  
155 ~~2015), the FireCCI51 and MCD64A1 products derived from TERRA&AQUA-MODIS (Giglio et al., 2018;~~  
156 ~~Lizundia-Loiola et al., 2020), the FireCCILT10 product derived from AVHRR (Otón et al., 2019) and the~~  
157 ~~C3SBA10 product derived from Sentinel-3 (Lizundia-Loiola et al., 2021). Currently, the MCD64A1 (collection~~  
158 ~~6), based on MODIS 500 m bands, is considered one of the most accurate global product (Chuvieco et al., 2019),~~  
159 ~~with omission and commission errors of 40% and 22% globally for the 'burned' class (Giglio et al., 2018). This~~  
160 ~~validation is based on independent globally distributed visually interpreted reference satellite data, however none~~  
161 ~~over Indonesia. These coarse-resolution datasets generally omit small-scale fires and, thus, the reported burned~~  
162 ~~area is underestimated (Ramo et al., 2021). This has motivated research in the use of medium-resolution satellites~~  
163 ~~(10 to 30 meters) such Sentinel-1 (Lohberger et al., 2018 in Indonesia), Sentinel-2 (Chuvieco et al. 2018 in Sub-~~  
164 ~~Saharan Africa), and the Landsat constellation (Hawbaker et al., 2017 in North America) to produce more detailed~~  
165 ~~burned area maps. Lohberger et al. (2018) reported 4.6 Mha burned in 2015 in Indonesia, nearly double the~~  
166 ~~estimate of 2.6 Mha from the Indonesian Ministry of Environment and Forestry (MOEF), using visual~~  
167 ~~interpretations of time-series Landsat-8 imagery (Sipongi, 2020).~~

168  
169 ~~For year 2019, The MOEF (hereafter 'Official estimate') estimated that 1.64 Mha burned in 2019 (Sipongi,~~  
170 ~~2020) Using visual interpretations of time series Landsat 8 imagery, the Indonesian Ministry of Environment and~~  
171 ~~Forestry (MOEF) estimated that 1.64 Mha burned in 2019 (Sipongi, 2020), while the MCD64A1 (collection 6)~~  
172 ~~indicated 2.03 Mha burned in 2019. The coarse 500-m spatial resolution MCD64A1 data omit smaller fires and~~  
173 ~~thus likely overlook many localized events. -The commonly used global MODIS annual burned area product~~  
174 ~~(MCD64A1, collection 6) (Giglio et al., 2018) indicated 2.01 Mha burning in 2019. Both datasets suffer~~  
175 ~~shortcomings that bias their estimates, however. The coarse 500 m spatial resolution MCD64A1 data omit smaller~~  
176 ~~fires and thus overlook many localized events and overestimate larger ones. The MCD64A1 dataset reports~~  
177 ~~omission and commission errors of 40% and 22% globally for the 'burned' class (Giglio et al., 2018). This~~

178 validation is based on independent globally distributed visually interpreted reference satellite data, however none  
179 over Indonesia. ~~The Conversely, the~~ Landsat imagery underlying MOEF estimates (hereafter ‘Official estimate’)  
180 ~~are the Official estimates are~~, while finer scale, observed every 16 days at best (typically much less due to cloud  
181 and smoke), meaning that many burn~~s-sears~~ may remain undetected. Also, smaller-scale and/or dispersed fire  
182 activity may be underestimated, considering the challenges of their visual interpretation and delineation. Visual  
183 interpretation entails a manual delineation of burn-sears perimeters, which yields accurate results for large burn  
184 sear mapping at local scales, but is very time consuming at large spatial scales, particularly when mapping small  
185 fires. A thorough accuracy assessment is also not available for the official burned-area products. Given the  
186 unknown errors around burned-area estimates, and the differences between them, the accuracy, and merits of ~~the~~  
187 different mapping approaches over Indonesia require formal examination.

188  
189  
190  
191  
192 Here, we present new and validated 2019 burned-area estimates for Indonesia using a time-series of the  
193 atmospherically corrected surface reflectance multispectral images (level 2A product) taken by the Sentinel-2 A  
194 and B satellites. With higher spatial resolution (20-m) and more frequent observations (5-day revisit time), the  
195 Sentinel-2A and B satellites offer relatively comprehensive and accurate burned-area mapping (Huang et al., 2016;  
196 Ramo et al., 2021). ~~As detailed below, w~~We ~~developed our method used~~ing the Google Earth Engine (Gorelick  
197 et al., 2017), ~~in turn allowing for its reproduction thus permitting wide application for ongoing burned area~~  
198 monitoring. We also developed an independent reference dataset to compare the accuracy of our estimate against  
199 the Official and MCD64A1 burned-area maps. Given the lack of ~~randomly objectively~~ distributed ground  
200 ~~verifications of ‘burned’ and ‘unburned’ locations~~truthing, we sought ~~an efficient way~~s to extract reference sites  
201 by visually detecting ~~either~~ a smoke plume, ~~a burn-sear~~, or ~~a~~ heat source (flaming front, or hotspot) from the  
202 archive of original ~~Sentinel-2 time series Sentinel-2~~ images. Finally, we examined differences in terms of  
203 ~~sear~~burn-size frequency distributions among these three burned-area estimates to examine spatial patterns.

## 205 2. Methods

### 206 2.1. Summary of methods

207 A burned area is ~~an area of land characterized identified by alteration of vegetation cover and structure by along~~  
208 with deposits of char and ash, ~~and by alteration of vegetation cover and structure~~. We mapped ~~burned such~~ areas  
209 using a change- ~~detection~~ approach, i.e. by comparing Sentinel-2 infrared signals recorded before and after a  
210 burning event (Liu et al., 2020). We ~~analyzed a time-series of the Normalized Burned Area Ratio (see section 2.2)~~  
211 to assemble two national composite images depicting ~~the spectral condition of~~ vegetation ~~shortly eondition~~  
212 before and ~~shortly after damage~~a disturbance (Figure 1). These composites represent a convenient way to capture  
213 ~~the entire burned landscape stored in just two image files. 2019 burning (Figure 1)~~Although we refer to these  
214 ~~images as “pre- and post-fire composites”, they also capture vegetation damage caused by automatically extracting~~  
215 pairs of nominally ‘burned’ and ‘unburned’ pixels from 47,220 original Sentinel-2 images acquired between 01  
216 November 2018 and 31 December 2019. by fire and by due to other causes, for example a cutting event (e.g.  
217 mechanical conversion to agriculture, to timber plantation, to roads, population centers, mining or natural timber  
218 harvesting), a disease, strong winds, floods, or landslides (Gaveau et al., 2021). ~~This reconstructed pair of pre-~~

219 ~~and post fire images spans the entire 2019 burning season. It is a convenient way to capture the entire burned~~  
220 ~~landscape stored in just two image files. Subsequent to~~After the production of ~~this image pair~~the pre- and post-  
221 ~~fire composites, we used a “Random Forest” classification model (see section 2.3) trained on visually identified~~  
222 ~~pairs of pre- and post-fire pixels to confirm if the spectral changes indicating vegetation damage corresponded to~~  
223 ~~a burning event. classified pixels of the pair as ‘burned’ or ‘unburned’ using a Random Forest classification model~~  
224 ~~trained on visually identified pairs of pre and post fire pixels.~~Third, three independent interpreters assembled a  
225 reference dataset by visually ~~interpreting~~identifying ~~burns~~sears in the original time-series (~~5-day repeat pass~~)  
226 Sentinel-2 images. Fourth~~and finally~~, we assessed our burned-area map, as well as the Official and MCD64A1  
227 burned-area maps, against our reference dataset to gauge the reliability and accuracy of the three burned-areas  
228 products. Finally, we tested whether, and how, the three burned-area estimates differed in their tendencies to  
229 incorporate burn~~sears~~ of ~~larger or smaller~~different sizes.

## 231 2.2. Pre- and post-fire Sentinel-2 national composite images of 2019

232 Here, we describe our automated procedure to ~~create a national pair of pre- and post-fire composites. extract pairs~~  
233 ~~of ‘burned’ and ‘unburned’ pixels~~from 47,220 ~~original~~ Sentinel-2 images acquired ~~throughout 2019. between 01~~  
234 ~~November 2018 and 31 December 2019. This set of pixel pairs was used to create the national composite pre and~~  
235 ~~post fire images and guide subsequent supervised classifications of burned areas nationally.~~ Prior to ~~running this~~  
236 ~~procedure~~creating the composites, we removed ~~cloud impacted~~non-valid pixels using the Sentinel-2 imagery  
237 quality flag (this flag provides information about clouds, cloud shadows, and other non-valid observations)  
238 produced by the ATCOR algorithm and included in the atmospherically-corrected surface reflectance  
239 multispectral images of the Sentinel-2 A and B satellites Surface Reflectance products (Level 2A product)  
240 (Fletcher, 2012).

241 A ~~time series of the Normalized Burned Ratio (NBR), given as  $(NIR-SWIR) / (NIR+SWIR)$ , represents a~~  
242 convenient index to detect ~~if and when~~the approximate day when the vegetation was damaged. ~~a disturbance in~~  
243 ~~the vegetation occurred in 2019, such as a burning event (Key and Benson, 1999).~~ Before ~~damage~~a fire, vegetated  
244 pixels register high NBR values close to 1 because reflectance in near-infrared spectrum (NIR; wavelength=0.842  
245  $\mu\text{m}$ ; Band 8) is high due to the chlorophyll content of the vegetation (open circles before ~~a disturbance. in this~~  
246 ~~case a fire.~~ in Figure 2). The NBR of ~~burned-damaged~~ vegetation typically ~~declines abruptly~~ towards 0 (or  
247  ~~$\leq 0$  for severe damage) because the NIR reflectance declines~~ due to chlorophyll and leaf destruction, ~~while the~~  
248 ~~reflectance of short-wave-infrared spectrum (SWIR; wavelength = 1.610  $\mu\text{m}$  or 2.190  $\mu\text{m}$ ; Band 11 or Band 12)~~  
249 ~~increases due to dead or charred material and exposed ground cover.~~ ~~such that~~ NBR values  ~~$\leq 0$  or  $\leq 0$~~  are often  
250 apparent for ~~a several few~~ weeks ~~after a fire severe burning or clear-cutting.~~ ~~while the reflectance of short wave~~  
251 ~~infrared spectrum (SWIR; wavelength = 1.610  $\mu\text{m}$  or 2.190  $\mu\text{m}$ ; Band 11 or Band 12) increases due to charred~~  
252 ~~material and exposed ground cover.~~ We analyzed ~~a~~ NBR time series ~~for~~ approximately 94.5 billion 400 m<sup>2</sup> pixels  
253 pairs (Indonesia’s landmass =198 Mha) ~~to detect the day when a pixel’s vegetation was disturbed by fire.~~ ~~We~~  
254 ~~describe the procedure to detect drops in the NBR time series in the following paragraph.~~

255 We detected ~~breaks~~drops in NBR time series with a moving-window approach. ~~Every two days, a~~ moving  
256 window scanned NBR values three months prior and one month after the central day of the window. The output  
257 value of the moving window (blue dots in Figure 2) is the difference ~~between~~ average NBR values observed  
258 before and after the central day. ~~The NBR average after the central day also included the value of~~at the central

259 day. The difference between the average NBR values was estimated every 2 days in the time series, skipping the  
260 day of year that was an odd number (day of year equal to 2, 4, 6, 8...). Although ~~the~~ Sentinel-2 has a temporal  
261 resolution of 5 days, the overlap between satellite passes may increase the temporal resolution regionally up to 2  
262 days ~~in~~ at the equator. Thus, we estimated the NBR difference (dNBR) every 2 days instead of -5 days. Taking this  
263 into consideration, our ~~burn~~ ‘disturbance’ date estimate has a maximum temporal precision of 2 days in specific  
264 regions, but generally 5 days when satellite passes do not overlap. The day of the year when ~~this~~ dNBR difference  
265 reached a maximum corresponded to the moment NBR dropped most markedly in each pixel ~~over a two-day~~  
266 ~~period~~, flagging a disturbance to the pixel’s vegetation potentially caused by fire. At this date, we created a pair  
267 of pre- and post-fire pixels by selecting the median Red, NIR and SWIR spectral values acquired three months  
268 before and one month after ~~the disturbance~~ ~~the potential burning event~~. We selected a one-month window rather  
269 than a three-month window to compute the post-fire image to maximize our chances to detect ~~a fresh-recent~~ burns  
270 ~~sears~~, given that burned areas on degraded lands and savanna tend to re-green rapidly. ~~We repeated this procedure~~  
271 ~~for approximately 94.5 billion pixels to assemble two national composite images depicting the spectral condition~~  
272 ~~of vegetation shortly before and shortly after a disturbance (Figure 1).~~

### 273 2.3. Supervised burned/unburned classification.

274 We used the Random Forest supervised classification algorithm (Breiman, 2001), available via the Google Earth  
275 Engine, to ~~determine whether the spectral changes detected by the pre- and post-fire composites corresponded to~~  
276 ~~a burning event, and subsequently~~ classify burned areas ~~from the pair of pre- and post-fire image composites~~  
277 ~~created above~~. Supervised classifiers require ‘training data’, that is, exemplary spectral signatures of ‘burned’ and  
278 ‘unburned’ lands in the present case, to guide the algorithm to reliably classify the target classes. The spectral  
279 signatures (i.e., the reflectance values in the pre- and post-fire composite images) are the predictive variables of  
280 the classification model. ~~Concretely,~~ ~~†~~ The features used in the Random Forest are the original bands of Sentinel-  
281 2 in the pre- and post-fire composites plus their respective NBR index. We excluded the bands at 60-meter spatial  
282 resolution (bands B1, B9, and B10) since these bands present a low spatial resolution for the aim of the study.  
283 Therefore, we used a total of 22 features: the NBR and bands B2, B3, B4, B5, B6, B7, B8, B8A, B11, and B12 of  
284 the pre and post-composites. ~~We used the NBR and all available Sentinel 2 spectral bands of the pre- and post-fire~~  
285 ~~image composites as input to the Random Forest model.~~

286  
287 We used a 10-fold cross-validation to assess the accuracy obtained with a set of different parameters in the  
288 Random Forest. The splitting ‘train-test’ in the cross-validation was done only with the training dataset, since the  
289 reference dataset used for the final validation must be completely independent of the training and model  
290 parametrization. The two parameters that we tuned were the *number of trees* and the *minimum leaf size*. Random  
291 Forest is an ensemble classifier composed of several Decision Trees; the parameter *number of trees* represents the  
292 number of Decision Trees in the Random Forest. The *minimum leaf size* represents the minimum number of  
293 samples that result from a splitting node at the Decision Tree. We found that a *minimum leaf size* equal to 1  
294 performed the best on average and, thus, we used this value. We selected a conservative *number of trees*, 50, to  
295 ensure the good performance of the Random Forest. We did not set any limit to the maximum nodes in each tree  
296 and the variable to split in the random forest was set to the square root of the number of variables, which is the  
297 common practice among machine learning practitioners and the default configuration in Google Earth Engine.



299 The required number of points used to train our supervised classification model (here a Random Forest) depends  
300 on the spectral separability of the classes (in our case two classes: “burned” and “unburned”). The pixels that  
301 show the burn ~~scar~~ present a singular spectral signature and, for this reason, it is necessary to collect a large  
302 amount of training points. We collected training points until we were satisfied with the results of the classification  
303 by visually comparing the resulting burned area map against the pre- and post-fire composites. We trained the  
304 Random Forest algorithm using 988 independent training pixels (Supplementary Figure S1 for locations), being  
305 point coordinates labelled as either ‘burned’ (317 points) or as ‘unburned’ (671 points). ~~The selection of these~~  
306 ~~pixels was/were selected/realized~~ by visual interpretation of the pre- and post- fire image composites. Burned  
307 areas show a distinctive dark (low albedo) brown/red color in the SWIR-NIR-Red composite image when  
308 displayed as Red-Green-Blue channels (Figure 1). The training pixels were collected ~~in a variety of across~~  
309 landcover types (Supplementary Table S1 for landcover types) to ensure the representativeness of the training  
310 dataset and the satisfactory generalization of the classification model across Indonesia. We selected training pixels  
311 focused explicitly on medium-to-high burn severity, i.e. areas where the distinctive red color in the SWIR-NIR-  
312 Red composite image looked the darkest, indicating that all or most of the vegetation/soil burned. This aspect of  
313 the methodology ~~hedged against over-estimation of total burned area by minimizing so-called ed~~ “false positives”:  
314 ~~It may however but may~~ exclude areas with implied low-burn severity ~~or low-visibility impacts~~, such as  
315 understory fires (below an intact forest canopy, see e.g., van Nieuwstadt and Sheil, 2005) ~~and even some~~  
316 ~~agricultural and grassland fires~~. By prioritizing confident identification of fires over absolute burned-area  
317 coverage, as well as by duly validating our estimates, this ~~conservative~~ approach ~~has the advantage of assuaging~~  
318 ~~sensitivities concerning~~ avoids the problems caused by frequent false positives (Rochmyaningsih, 2020).

319 We assessed burn severity during ~~algorithm~~ training based on visual interpretation. RGB composites with bands  
320 11 (SWIR wavelength = 1.610  $\mu\text{m}$ ), 8 (NIR wavelength=0.842  $\mu\text{m}$ ) and 4 (RED wavelength = 0.665  $\mu\text{m}$ ) provide  
321 information about the severity of the fire; burn ~~scars~~ with high severity present a dark (low albedo) red/brown  
322 color (Figure 1). We included the histogram of dNBR ( $\text{NBR}_{\text{postfire}} - \text{NBR}_{\text{prefire}}$ ) for the 317 training points labelled  
323 ‘burned’ in Supplementary Figure S2 to corroborate that the ‘burned’ training samples were selected in areas with  
324 medium to high severity fires. Eighty one percent (256) of ‘burned’ training points (317) had dNBR values  
325 ( $\text{NBR}_{\text{postfire}} - \text{NBR}_{\text{prefire}}$ ) < - 0.44, which represents the threshold for medium to high severity burns according to the  
326 proposed classification table of the United States Geological Survey (USGS).

#### 329 2.4. Burned-area map validation.

330 The Gold standard is to validate the map against a sufficiently large reference dataset developed based on ground  
331 visits to ‘burned’ and ‘unburned’ sites sampled ~~randomly objectively and randomly~~ across the ~~country region of~~  
332 interest (Olofsson et al. 2014). We sought ~~another alternative ways~~ to generate the reference dataset because the  
333 sample of GPS locations of ‘burned’ locations collected by Indonesian government were not available. Given the  
334 laborious scale of this validation exercise, we validated our burned-area estimates for only the seven provinces  
335 prioritized by the Indonesian Government for restoration of fire-prone degraded lands (Kalimantan Barat,  
336 Kalimantan Tengah and Kalimantan Selatan, Papua, Jambi, Riau, and Sumatra Selatan). These provinces are also  
337 those that typically burn most extensively. We used visual interpretations of the original time-series Sentinel-2  
338 imagery acquired every 5 days over 2019 at 1298 randomly selected sites (one site = one pixel of 20 m x 20 m)

339 to detect flaming fronts (fire hotspots) and other signs of burning (smoke and charred vegetation). We used these  
340 reference data to calculate the overall accuracy (OA), producer's accuracy (PA), and user's accuracy (UA) with a  
341 95% confidence interval, of all three burned area maps (i.e., our Sentinel-derived burned-area classification, the  
342 official Landsat-based burned-area map, and the MCD64A1 product) following "good practices" for estimating  
343 area and assessing accuracy reported by Olofsson et al. 2014. We use the term '*mapped burned-area*' for the area  
344 classified as burned by each burned-area map. We employ the term '*corrected burned-area*' for the estimation of  
345 the burned area based on the validation of a given burned-area map against the reference dataset, following the  
346 practices in Olofsson et al. 2014. For instance, a high omission rate in the 'burned' class of a given burned-area  
347 estimate would potentially lead to a lower *mapped area* than a *corrected area* for that estimate, while a high  
348 commission rate would potentially lead to a higher *mapped area* than the *corrected area*. The *corrected area*  
349 represents an estimation of the actual burned area for year 2019 computed for each of the three datasets separately.  
350 The accuracy of the burned area map, and the sample size of the reference dataset, play a role in the confidence  
351 interval of *corrected area* estimate. Lower map accuracy and smaller sample size mean wider confidence  
352 intervals.

353

#### 354 2.4.1. Reference site sampling design

355 ~~The~~ Good practices for estimating area and assessing accuracy, ~~as~~ reported in Olofsson et al. (2014), assumes a  
356 simple random sampling or a stratified random sampling in the generation of the reference dataset. In our case  
357 study, we employed a stratified-random sampling approach to ensure an acceptable sample of 'burned' reference  
358 sites. Our stratified approach was necessary given that the 'burned' class was rare over the study area: the area  
359 of seven provinces of interest is 87.6 Mha and the combined area detected as burned by all three datasets  
360 represented only 3.1% of this area.

361 For the generation of the 1298 reference sites ([see Supplementary Table S4 for associated landcover types one](#)  
362 [year before fire](#)), we ~~first~~ randomly sampled (i) 419 sites across from the areas classified 'burned' by the three  
363 datasets (red area in Figure 3a; Supplementary Table S24), and (ii) 879 sites in areas classified as 'unburned' by  
364 all three datasets hereafter denoted U (grey area in Figure 3a). This sample size is deemed sufficient and  
365 comparable to other map assessments at larger scale (Stehman et al., 2003; Olofsson et al., 2014).

366 This initial sample of 1298 total sites present a shortcoming for direct pair-wise comparisons of between the  
367 reference dataset and each of the three burned-area maps individually. Specifically, sampling densities in the  
368 reference dataset were far greater in areas classified 'burned' by the three datasets (red area in Figure 3a) compared  
369 to the area deemed 'unburned' by all three datasets, hereafter denoted U (grey area in Figure 3a). Consequently,  
370 for the validation of a given burned-area dataset, its total number of 'unburned' reference sites would be over-  
371 sampled upon defining 'unburned' reference sites with reference to U as well as areas classified as burned uniquely  
372 by one of the other two maps (cyan areas in Figure 3b, c, d, hereafter denoted as U'). Such over-sampling of  
373 reference sites in the realm of U' would violate the stratified-sampling approach described in Olofsson et al.  
374 (2014) and would lead to an erroneous accuracy assessment. ~~In order to~~ To achieve a balanced stratified sampling  
375 of reference sites across 'burned' and 'unburned' areas of each dataset, we generated three subsamples from the  
376 initial 1298 reference sites (red areas in Figures ~~4f, 3e, g, h, g~~) and used these subsamples to validate each dataset.  
377 These three subsamples were generated by randomly excluding reference sites from the realm of U' in Figure 3b,  
378 c and d, respectively, until the density of reference sites in U' equaled the density of the larger unburned area U.

379 For instance, for the validation of the Official burned-area map, the density of reference sites in U was 10.36  
380 sites/Mha, and the extent of U' was 1.551 Mha, such that the number of reference sites to retain in U' for this  
381 validation was given as 1.551 Mha x 10.36 sites/Mha = 16 sites. The calculations of the number of sites removed  
382 from each subsample are illustrated in Supplementary Table S32. The final, adjusted, stratified subsamples of  
383 reference sites used for validation is given in Table 1.

384

385

386

387

388

389

#### 390 2.4.2. Interpretation of the burned-area reference dataset

391 We developed a series of scripts in the Google Earth Engine to streamline the visual interpretation of the reference  
392 sites. Specifically, we adapted a script written by (Olofsson et al. 2014) to rapidly scan the time-series of original  
393 Sentinel-2 images in visible and infrared bands and thus visually detect either a smoke plume, a burn ~~scar~~, or a  
394 heat source (flaming front), and determine whether and when in 2019 a reference site burned. The script enabled  
395 the interpreter to interactively track the evolution of NBR values and patterns over the 2019 time series of 5-day  
396 images. Reference sites were investigated for burning wherever a marked drop in the NBR time series was  
397 detected, indicating a disturbance in the vegetation. For reference sites where a disturbed area was observed, we  
398 subsequently reviewed the last few images before the drop in NBR and the first few images after the drop.  
399 Interpreters looked for three distinct signs of burning in these images to confirm them as burned: (i) smoke plumes;  
400 (ii) flaming fronts – that is, a line a moving fire where the combustion is primarily flaming; and (iii) rapid changes  
401 in color from 'green' to 'dark red', characteristic of a transition to charred vegetation (Figure 4). ~~If rapid changes~~  
402 ~~in color were observed over the reference site, with at least one direct feature (smoke or flame) in its vicinity, this~~  
403 ~~indicated a fresh burn scar, and the reference site was declared 'burned'. If rapid changes in color were observed~~  
404 ~~over the reference site, with at least one direct feature (smoke or flame) in its vicinity, this indicated a fresh burn~~  
405 ~~scar, and the reference site was declared 'burned'. If rapid changes in color from 'green' to 'dark red' were~~  
406 ~~observed without smoke or flame, the reference site was also declared 'burned'. If no change in color was~~  
407 ~~observed, with at least one direct feature (smoke or flame) in its vicinity, the reference site was declared~~  
408 ~~'unburned'. If none of these three features were observed, the reference site was declared 'unburned'.~~

409

410

411 Three interpreters independently reviewed the time-series of original Sentinel-2 images and associated NBR  
412 trends for all reference sites (N=1298) (see Supplementary Figure S3 for a frequency distribution of burn scar  
413 sizes of the Sentinel-2 burned-area map, for select spatially coincident 'burned' reference sites). To reduce  
414 uncertainties associated with the interpretation of the imagery, the results of the three interpreters were compared  
415 to each other. If all three interpreters recorded the same interpretation and timing of a burning event for a given  
416 reference site, their interpretations were retained. If one or more interpreters disagreed, all interpreters reviewed

417 the data and resolved discrepancies by consensus. In some cases, it was difficult to reconcile disagreements  
418 because of poor image quality or because of uncertain spectral patterns. Therefore, if possible, interpreters also  
419 explored other satellite images (e.g. Landsat) to detect the presence of fire and resolve disagreements for a given  
420 reference site. The sites in which the three interpreters disagreed were ultimately excluded (70 sites) from the  
421 reference dataset. For these excluded sites, disagreement typically resulted from uncertainties over the boundary  
422 of burned or unburned areas, or because the imagery was not clear enough. The ~~final~~-sample size of reference  
423 points explored here, N=1298, excludes the discarded points of disagreement in question.

424 We created a second script to generate snapshot images (see examples in Figure 4) depicting infrared spectral  
425 conditions, shortly before and shortly after a fire, as well as the corresponding image dates. Interpreters recorded  
426 and geotagged a snapshot of before and after fire condition at every reference site (for which a burned area was  
427 detected) to enable third-party reviewers to check the consistency and validity of interpretations on site-by-site  
428 basis (See Data Availability).

429

#### 430 2.4.3. *Burn ~~scar~~-size comparisons.*

431 We tested whether, and how, the three burned-area estimates differed in their tendencies to incorporate burn-~~scars~~  
432 of larger or smaller sizes. Specifically, we compared the frequency distributions of burn-~~scar~~ size-areas (or  
433 “scars”) amongst the three estimates to test for similarity and qualify any distinguishing differences on the part of  
434 our Sentinel-based estimate. Differences amongst burn-~~scar~~ size frequency distributions implies that a given  
435 burned-area estimate is ~~more or less inclusive~~inclusive of burn-~~scars~~ of a given size, regardless of absolute  
436 differences to total burned area between the estimates. Inter-estimate comparisons of burn-scar size frequency is  
437 analogous to tests of whether the ‘samples’ of burn-~~scars~~ defined by each estimate describe the same, ultimately  
438 partially-observed universe of fire activity. Significant inter-estimate differences imply greater or lesser inclusion  
439 of a given realm of fire activity – e.g., small-scale agricultural burning, plantation fires, extreme wildfires – thus  
440 indicating bias (or lack thereof) without defining such realms explicitly.

441 For all three estimates, we employed the Kruskal-Wallis H test of differences with respect to the ‘location’ of  
442 frequency distributions along a continuum of burn-~~scar~~ sizes. Given significant inter-estimate differences  
443 according to this three-way test, we tested for two-way differences in the shape and location of the ~~scar~~burn-size  
444 frequency distribution (Kolmogorov-Smirnov test), as well as two-way differences in medians (Mann-Whitney U  
445 test), between our Sentinel estimate and either the Official or MODIS estimate individually. ~~We performed all~~  
446 ~~comparisons for scar~~burn ~~size cohorts > 6.25 ha, > 20 ha, > 100 ha, > 1000 ha, and > 5000 ha, without Bonferonni~~  
447 ~~correction given the nested nature of these cohorts.~~ Testing for similarity over increasingly large scar-size cohorts  
448 clarified the degree to which significant inter-estimate differences were attributable to the inclusion or omission  
449 of a given cohort.

450

451 We excluded ~~scars~~burns <6.25 ha because this is the minimum observable burn-~~n-scar~~-size ~~according to MODIS~~  
452 ~~data, given pixel resolution, and it is already evident that our Sentinel estimates are distinguished by their ability~~  
453 ~~to detect burn scars below this threshold. The of the~~ Landsat-8 Official estimates ~~similarly have few scars < 6.25~~  
454 ~~ha~~ due to the challenging nature of visual interpretations at such ~~fine~~ scales. We note that the minimum scar-size  
455 of the MODIS data is 25 ha, hence for comparison with MCD64A1 product we used a 25-ha threshold. In relation  
456 to Sentinel and MODIS estimates, for which burned areas were originally mapped as arrays of pixels, we defined

457 a burn ~~sear~~ to be any array of pixels contiguous across cardinal directions but not diagonals to render the resultant  
458 burned-area map conservative with respect to patch size (Figure S4).— For the Official estimate, burns ~~sears~~ are  
459 as manually delineated via visual interpretation by interpreters from the Government of Indonesia. All ~~sears~~-burns  
460 are spatially and temporally discrete, such that ~~sears~~-burns of a given estimate that overlap spatially but not  
461 temporally are considered separate.

462

### 463 3. Results

464

#### 465 3.2. Increased Burned-Area Estimates

466 Our Indonesia-wide burned-area estimate, based on the classification of the pair of pre- and post-fire Sentinel-2  
467 composites, are larger than the Official estimates as well as the MODIS MCD64A1 to a lesser degree. We estimate  
468 3.11 million hectares (Mha) burned in 2019 across Indonesia, of which 31% were on peat (Figure 5). The extent  
469 of peatlands were defined using a national dataset from the Ministry of Agriculture (Ritung et al., 2011). In  
470 contrast, Official burned-area estimates, based on visual interpretation of Landsat-8 imagery, report only about  
471 half as much burned area, at 1.64 Mha, of which 39% was on peat. Our estimates too are similarly considerably  
472 greater than the MODIS MCD64A1 product, which reports 2.04 Mha burned in 2019, or two-thirds of our  
473 estimate, with 40% on peat. The greater burning extent and proportionally lesser extent of peatland burning  
474 according to our estimates suggest that our estimates are particularly more inclusive of burning across mineral  
475 soils.

476

477 In the seven provinces for which we ~~carried out the assessed~~ accuracy ~~assessment~~, our Sentinel-2 estimates, and  
478 the Official Landsat-8 estimates both report excellent user's accuracies (UA) for the 'burned' class, at 97.9% (CI:  
479 97.1%-98.8%) and 95.1% (CI: 93.5%-96.7%) respectively, indicating a mere 2.9%-4.9% commission-error rate  
480 (Table 2, Supplementary Table S53). The producer's accuracies (PA) are comparatively lower for both datasets,  
481 but notably less so for our estimates, at 75.6% (CI: 68.3%-83.0%) and 49.5% (CI: 42.5%-56.6%) for our estimate  
482 and the Official dataset, respectively. In other words, for any burned area in our reference dataset, there is a 75.6%  
483 chance that it will be correctly mapped as burned by our estimate, compared to only a 49.5% for the official  
484 estimate. This is in keeping with the greater tendency of the Sentinel-2 estimate to capture more smaller and  
485 intermediate-size burn ~~sears~~. The MCD64A1 data had a much lower UA for the burned class, at 76.0% (CI:  
486 73.3%-78.7%), as well as a much lower and a PA for the burned class, at 53.1% (CI: 45.8%-60.5%), qualifying it  
487 as the least reliable and accurate of the three estimates notwithstanding comparable high overall accuracy (Table  
488 2).

489 All three burned-area maps underestimate the true burned area extent, as per their respective PA figures, but our  
490 Sentinel-based map underestimates considerably less severely has the smallest shortfall without a corresponding  
491 loss of and also maintains user's accuracy. The corrected burned area of the seven provinces is higher than the  
492 mapped area for all the three burned area maps. Again, however, our ~~Sentinel-based~~ map area most closely  
493 approximates its corresponding corrected burned area (Table 2). Whereas our Sentinel-based mapped burned area  
494 indicates that 1.84 Mha burned in the seven provinces (or 59% of our total national estimated burned area), the  
495 corrected burned area is 2.38 Mha (CI: 2.14 Mha-2.61 Mha) (Table 2), for a discrepancy of 0.54 Mha. In contrast,

496 the official estimate indicates 1.19 Mha burned in the seven provinces (73% of its corresponding total), and a  
497 corrected burned area of 2.29 Mha (CI: 1.96 Mha-2.63 Mha), for a 1.1 Mha discrepancy. Likewise, the MCD64A1  
498 dataset mapped 1.58 Mha burned in the seven provinces and has a corrected burned area of 2.27 Mha (CI: 1.94  
499 Mha-2.59 Mha), for a 0.69 Mha discrepancy. Although, we cannot extrapolate a corrected burned area across  
500 Indonesia, we ~~are~~ confidently ~~conclude~~ that appreciably more than 3.11 Mha burned nationally in 2019.

### 501 3.1. Burn ~~scar~~ size comparison.

502 The Sentinel, Official and MCD64A1 estimates captured significantly distinct realms of fire activity, as  
503 represented by ~~their~~ relative burn size frequencies of ~~scar sizes~~ (Figure S62). The three estimates differ from one  
504 another ~~decreasingly over increasingly larger minimum scar size thresholds~~ most notably for small burns,  
505 however, ~~and they~~ are statistically indistinguishable for ~~scars~~ burns > 5000 ha indicative of extreme fire activity  
506 (Table 3). In other words, all three estimates capture very large ~~scars~~ burns (>5000 ha) equally well, and  
507 distinctions amongst the estimates concentrate amongst small (<100 ha), intermediate (100-1000 ha) and larger  
508 burns (1000-5000 ha) ~~scars~~, in decreasing order of degree as indicated by the magnitude of the test statistics in  
509 Table 3.

510

511

512 Inclusivity of smaller and intermediate ~~scars~~ burned areas is the primary source of difference among estimates.  
513 Compared to Official or MCD64A1 estimates, the Sentinel estimate has a significantly greater relative frequency  
514 of small ~~scars~~ burned areas (< 100 ha), especially amongst the smallest of these ~~scars~~ (Table 4). This is indicative  
515 of a greater detection of ~~the realm of fire activity~~ small fires presumably characterized by small-scale agriculture  
516 fires and similar, small-scale controlled burning. The Sentinel estimate similarly has a greater relative frequency  
517 of intermediate ~~scars~~ sized burns (100-1000 ha), but less acutely so, with inter-estimate differences being more  
518 moderate for the Official estimate than the MCD64A1 estimate (Table 4, Figure 6, Figure S62). For ~~scars~~ burns  
519 >1000 ha, the Sentinel estimate differs only relative to the official estimate (Table 3), seemingly due to the latter's  
520 ~~lesser estimation~~ underestimation of large and very large scars (Figure 6). Note for instance the increasingly large  
521 divergence between the cumulative burned-area curves for the Sentinel-2 and the Official estimates in Figure 6  
522 for ~~scars~~ burn areas > 1000 ha. For very large ~~scars~~ burns (> 5000 ha), two-way comparisons in Table 4 again  
523 report no significant statistical differences in burn-scar detection rates between the Sentinel and alternative  
524 estimates. However, given the small sample of patches > 5000 ha, it is noteworthy that the Sentinel estimate  
525 captures more very large scars compared to Official estimates (n=56 vs n=16) and avoids critical omissions made  
526 by both Official, or MCD64A1, estimates for extremely large ~~scars~~ burns (>15,000 ha) on peatlands around  
527 Berbak National Park in Jambi Province, Sumatra (Figure 71, Inset A).

528

529 In summary, the greater overall burned-area estimate of our Sentinel data compared to the Official and MCD64A1  
530 alternatives is largely attributable to ~~reflects~~ differences in the inclusion of smaller and intermediately sized scars.  
531 ~~Indeed, the~~ aerial sum of all Sentinel burn ~~scars~~ areas that are individually <~860 ha equals the entirety of the  
532 official burned-area estimate (Figure 6). ~~The~~ We note that the Sentinel-2 estimate data exhibits a size-frequency  
533 pattern that approximates ~~the linear expectation of a near scale-free power-law~~ (Figure 6). ~~While the finer spatial~~  
534 ~~resolution of Sentinel data must account for some of the inter-estimate discrepancies, particularly relative to the~~

~~MCD64A1 estimate and scars burns < 100 ha (Figure S2), overall the discrepancies above seem more in keeping with our estimate's are dominated by greater different sensitivity detection of otherwise overlooked smaller-scale burnings smaller burns. Hence, the inter-estimate differences qualify our Sentinel estimates not simply as more extensive but also as qualitatively distinct in terms of the degree to which different realms of fire activity are captured. The near linear log-log frequency-area distribution over several orders of scar size of our Sentinel product as indicated by these a characteristic comparisons over a range of sizes power-law relationship (Figure 6).~~

#### 4. Discussion

We developed a method that generates two national composite Sentinel-2 images depicting vegetation condition before and after burning in 2019 (Figure 1), and then classified this pair to extract burned areas using a Random Forest supervised classification algorithm. We developed a comprehensive validation protocol to strictly assess the reliability and accuracy of our product based on visual interpretation of dense time-series Sentinel-2 original images, and also applied this validation to the widely used global MODIS burned-area product (MCD64A1, collection 6) (Giglio et al., 2018) and to the Official burned-area product of the Indonesian Ministry of Environment and Forestry (MOEF) (Sipongi, 2020).

Our estimate is the most reliable and accurate and therefore captures more of the 2019 total burned area, confirming that 20-m Sentinel-2 imagery is better suited to widespread small-scale agricultural burning in Indonesia (Huang et al., 2016), while it also captures large burn scars relatively thoroughly. The study finds similar omission and commission errors (47% and 24%) for the 'burned' class of MCD64A1 product as those presented globally (40% and 22%) (Giglio et al., 2018). The underestimation of total burned area according to the MCD64A1 product compared with our Sentinel-2 estimate is unsurprising, considering that the MODIS 500-m pixel resolution struggles to detect smaller fires (Giglio et al., 2018). Similar conclusions were reached by Ramo et al. (2021) when comparing the new 'Small Fire Dataset' derived using Sentinel-2 over Sub-Saharan Africa (Chuvieco et al., 2018) and the MCD64A1 product. More surprising is the near 2:1 ratio by which the Sentinel-2 estimates surpass the Landsat-8 Official estimate. Our examination shows that this difference reflects differential detection of small- (<100 ha) to intermediate-sized (<1000 ha) burn scars.

~~The burn-scar frequency distribution of the Sentinel-2 estimate is characteristic of robust power-law relation (Figure 6), a pattern typical of large-scale fire studies (Malamud et al., 1998). Modern studies suggest that these fractal-like patterns are often subtly more complex and can arise through a range of phenomena (Karsai et al., 2020; Falk et al., 2007). We note that the Sentinel-2 estimate data exhibits a size-frequency pattern that approximates closer to the linear expectation of a near scale-free power-law, or pareto distribution (Karsai et al., 2020; Falk et al., 2007). These patterns are typical of large-scale fire studies (Malamud et al., 1998). compared to either of the alternative burned-area estimates, both Both other methods yield of which show a clearly an S-shaped curve with less area at smaller and larger sizes than captured in the Sentinel-2, indicating the likely bias by omission over the entire range of scales and are not determined by image resolution alone (Figure 6). These results, with different frequency patterns arising from burns from the same regions in the same period, also highlight the danger in interpreting apparent burned-area patterns without careful consideration of the limitations and biases that arise from the methods used to map them—an issue that may not have always been sufficiently recognized in past assessments or policy.~~

Although both Sentinel-2 and Landsat-8 both observe the infrared wavelengths required to detect charred vegetation and have similar spatial resolutions (20 m x 20 m and 30 m x 30 m, respectively), Sentinel-2 detects

575 more burns of the greater frequency of its coverage (five- versus sixteen-day revisit time). Also, our method  
576 avails of the massive computational capabilities and automation of the Google Earth Engine, allowing us to  
577 analyze more images and thus map more and smaller burn scars and associated details than could even the most  
578 well-equipped team of visual interpreters.

579 Despite high reliability that every burn scar detected on the map was valid (2.9% commission error rate), our  
580 method suffered a 24.4% omission error rate (burned areas that remained undetected). These rates reflect  
581 necessary tradeoffs between commission and omission error in a context where conservative estimates are much  
582 preferred for environmental policy and monitoring. We prioritized a low commission error rate (i.e. high user's  
583 accuracy) over absolute burned-area coverage to address sensitivities (Rochmyaningsih, 2020). By hedging  
584 against commission errors, our approach omitted hard-to-detect events, including low-intensity burns, such as  
585 those that occur beneath the forest canopy on mineral soils (van Nieuwstadt and Sheil, 2005) or on savanna  
586 grasslands, which tend to re-green rapidly. While further work is required to clarify and refine the optimal levels  
587 of inclusivity and reliability, we emphasize that the production of before and after fire annual composite images  
588 is relatively straightforward for the user community, given the availability of both the necessary imagery and our  
589 Google Earth Scripts.

590 ~~We stress that while the accuracy assessment proved that our training dataset is valid for the classification of~~  
591 ~~Sentinel-2 composites for the year 2019 in Indonesia. The training dataset collected in this study, however,~~  
592 ~~might not show achieve equivalent the same accuracy results for other years and regions. The pre- and post-fire~~  
593 ~~composites might show different spectral changes for other years if conditions are different under different~~  
594 ~~conditions. For instance, we noted that the high rainfall was higher for their year 2020, which leads to~~  
595 ~~different influenced reflectance values in the composites. Similarly, representative training points should be used~~  
596 ~~in other regions. Those adapting these methods should ensure adequate local training data and validation. Thus,~~  
597 ~~the generalization of our algorithm for other years should consider additional training points that reflect a wider~~  
598 ~~range of spectral changes not considered in year 2019 (i.e. dry to wet peatlands for year 2020). Similarly, our~~  
599 ~~training dataset is only valid for Indonesia. A, and additional training points should be considered for the~~  
600 ~~classification of burned areas in other regions of the world since spectral changes might differ from our original~~  
601 ~~study.~~

602 ~~In the past considerable emphasis was placed on the necessity of ground checks to validate and calibrate remote~~  
603 ~~sensing based estimates. Sometimes commentators raise doubts about may persist concerning our ability to~~  
604 ~~confidently estimates of burn scars areas without extensive and costly on the ground ground truthing ground-~~  
605 ~~checks. Modern high-resolution remote sensing makes such on-the-ground checks less essential than in the past~~  
606 ~~as burned areas are readily identified with good accuracy in modern high-resolution imagery such as that we used~~  
607 ~~for our validation. The protocol developed here to generate a reference dataset based on visual inspection of dense~~  
608 ~~(5-day revisit time) satellite imagery is better suited than ground verifications of 'burned' and 'unburned'~~  
609 ~~locations, because it allows the generation of extensive randomly distributed randomly distributed well~~  
610 ~~characterised reference sites, a process too time-consuming and costly with field visits. The identification and~~  
611 ~~quantification of less-readily-detected burned areas, such as those under a closed forest canopy, remain a challenge~~  
612 ~~but will require dedicated and targeted research and would not be solved by ground-checks alone.~~

613 Accurate estimates of burned lands, in particular on peat, are central to address<sup>ing</sup> concerns about regional air  
614 quality, and to ambitious national climate-change atmospheric carbon reduction commitments heavily reliant on



615 improved land/fire management (DGCC, 2019). Though we observed proportionally less peatland burning than  
616 the alternative burned-area estimates (31% versus 39% and 40% for the Official and MCD64A1 products,  
617 respectively), due to our more complete coverage, we observed more peatland burning absolutely (0.96 Mha) than  
618 the official estimate (0.64 Mha). Given this large discrepancy for peatland burning, we anticipate that our  
619 ~~improved mapping approach~~ refined burned area product will become a “gold standard” reference ~~enable others to~~  
620 ~~better estimate to calculate~~ carbon emissions from the 2019 fires in Indonesia. Combined with daily fire hotspots  
621 detected using thermal remote sensing, our detailed burned-area map can help identify ignition sites and estimate  
622 fire duration more precisely, and therefore contribute to forensic analyses of burning across landholdings (~~e.g.~~  
623 ~~concession owners~~) (Gaveau et al., 2017) as well as assess policies and practices intended to reduce or control  
624 ignition events and the scale of fires (Watts et al., 2019).

625 The Indonesian government has shown some success in reducing fires (Sloan et al., ~~in review~~2021). Apparent  
626 reductions to fire activity would however ideally be qualified using our more inclusive and accurate burned-area  
627 estimates. Further, the Indonesian government must also develop improved protocols to quantify the resulting  
628 carbon emissions (DGCC, 2019). Our protocols for creating reliable ~~and accurate burned area maps~~ pre- and post-  
629 ~~fire composites~~ are replicable. To further the adoption and reproduction of our approach, we have published all  
630 our protocols, scripts, applications, burned-area map, reference data, pre-fire and post-fire Sentinel-2 composite  
631 images, and various other outputs so that anyone may employ and revise them as they wish (see Data Availability).

632

## 633 5. Code availability

634 The code that generates the Sentinel-2 pre- and post-fire composites can be found at:  
635 [https://github.com/thetreemap/IDN\\_annual\\_burned\\_area\\_detection](https://github.com/thetreemap/IDN_annual_burned_area_detection)

## 636 6. Data Availability

637 All the data including pre- and post-fire composites, all three burned area products, and reference points with  
638 screenshots can be visualized online at this application portal:  
639 <https://thetreemap.users.earthengine.app/view/burn-area-validation-simplified>

640 The Sentinel-based burned area map and reference dataset are freely available for download at:  
641 <https://doi.org/10.5281/zenodo.4551243>.

642 The dataset *2019\_burnedarea\_indonesia.shp* contains the 2019 burned-area estimates that we developed for  
643 Indonesia using 20 m x 20 m time-series Sentinel-2 imagery. The reference dataset *Reference\_dataset.shp*  
644 contains 1298 reference points that we assembled and used to validate all three burned area products described in  
645 this study. Each reference point includes attribute ‘REFERENCE’ to describe the values obtained by visual  
646 interpretation: either ‘NO’ unburned or ‘YES’ burned. Each reference point has three attributes: ‘C\_SENTINEL’  
647 ‘C\_OFFICIAL’ and ‘C\_MCD64A1’ to describe the values of the classification of each burned area product: either  
648 ‘NO’ unburned or ‘YES’ burned. Finally, each reference point has three additional attributes: ‘SENTINEL’,  
649 ‘OFFICIAL’, and ‘MCD64A1’ to describe which burned area product this reference point validates. The values  
650 are either 0: not validate or 1: validate.

651 The MODIS MCD64A1 dataset was obtained at: [https://developers.google.com/earth-](https://developers.google.com/earth-engine/datasets/catalog/MODIS_006_MCD64A1)  
652 [engine/datasets/catalog/MODIS\\_006\\_MCD64A1](https://developers.google.com/earth-engine/datasets/catalog/MODIS_006_MCD64A1). The official burned area dataset from the Ministry of  
653 Environment and Forestry (MOEF) was obtained at: <https://geoportal.menlhk.go.id/webgis/index.php/en/>  
654 The Sentinel-2 Level 2A used in this study are available at <https://scihub.copernicus.eu/> and can be retrieved in  
655 Google Earth Engine. The Sentinel- 2 data are hosted and accessed in the Earth Engine data catalog (the links to  
656 the data are [https://developers.google.com/earth-engine/datasets/catalog/COPERNICUS\\_S2\\_SR](https://developers.google.com/earth-engine/datasets/catalog/COPERNICUS_S2_SR)). Data ingested  
657 and hosted in Google Earth Engine are always maintained in their original projection, resolution, and bit depth  
658 (Gorelick et al., 2017).

659

660 **Financial support.** Funding by the CGIAR Research Program on Forests, Trees and Agroforestry (CRP-FTA),  
661 with financial support from the donors to the CGIAR Fund, is recognized.

662

663 **Author Contributions.** D.L.A.G. designed the study. DL.A.G, M.A.S. and A.D designed the burn scar detection  
664 method. M.A.S. and A.D wrote the code in Google Earth Engine. D.L.A.G, M.A.S. and A.D. carried out the  
665 validation. S.S. carried out the burn scar size analysis. D.L.A.G., A.D. S.S. and D.S. interpreted the results and  
666 wrote the manuscript and produced the figures.

667

668 **Competing interests.** The authors declare no competing interests. Readers are welcome to comment on the online  
669 version of the paper.

670

## 671 **References**

672 Adrianto, H. A., Spracklen, D. V., Arnold, S. R., Sitanggang, I. S., and Syaufina, L.: Forest and Land Fires Are  
673 Mainly Associated with Deforestation in Riau Province, Indonesia, *Remote Sensing*, 12, 3, 2020.

674

675 [Alonso-Canas, I., and Chuvieco, E.: Global burned area mapping from ENVISAT-MERIS and MODIS active fire  
676 data, \*Remote Sensing of Environment\*, 163, 140-152, 2015.](#)

677

678 Breiman, L.: Random forests, *Machine learning*, 45, 5-32, 2001.

679

680 Cai, W., Yang, K., Wu, L., Huang, G., Santoso, A., Ng, B., Wang, G., and Yamagata, T.: Opposite response of  
681 strong and moderate positive Indian Ocean Dipole to global warming, *Nature Climate Change*, 11, 27-32,  
682 10.1038/s41558-020-00943-1, 2021.

683

684 Carmenta, R., Zabala, A., Trihadmojo, B., Gaveau, D., Salim, M. A., and Phelps, J.: Evaluating bundles of  
685 interventions to prevent peat-fires in Indonesia, *Global Environmental Change*, 102154, 2020.

686 Cochrane, M. A.: Fire science for rainforests, *Nature*, 421, 913-919, 2003.

687

688 [Chuvieco, E., Mouillot, F., van der Werf, G. R., San Miguel, J., Tanase, M., Koutsias, N., García, M., Yebra, M.,  
689 Padilla, M., and Gitas, I.: Historical background and current developments for mapping burned area from satellite  
690 Earth observation, \*Remote Sensing of Environment\*, 225, 45-64, 2019.](#)

691

692 [Chuvieco, E.; Pettinari, M.L.; Bastarrrika, A.; Roteta, E.; Storm, T.; Padilla Parellada, M.: ESA Fire Climate  
693 Change Initiative \(Fire\\_cci\): Small Fire Dataset \(SFD\) Burned Area pixel product for Sub-Saharan Africa, version  
694 1.1. Centre for Environmental Data Analysis, 12 October 2018, 2018,  
695 doi:10.5285/065f6040ef08485db989cbd89d536167.](#)

696  
697 Crippa, P., Castruccio, S., Archer-Nicholls, S., Lebron, G., Kuwata, M., Thota, A., Sumin, S., Butt, E.,  
698 Wiedinmyer, C., and Spracklen, D.: Population exposure to hazardous air quality due to the 2015 fires in  
699 Equatorial Asia, *Scientific reports*, 6, 1-9, 2016.  
700  
701 Dennis, R. A., Mayer, J., Applegate, G., Chokkalingam, U., Colfer, C. J. P., Kurniawan, I., Lachowski, H., Maus,  
702 P., Permana, R. P., and Ruchiat, Y.: Fire, people and pixels: linking social science and remote sensing to  
703 understand underlying causes and impacts of fires in Indonesia, *Human Ecology*, 33, 465-504, 2005.  
704  
705 DGCC: Emission Reduction Report, Directorate General of Climate Change, 2019.  
706  
707 Falk, D. A., Miller, C., McKenzie, D., and Black, A. E.: Cross-scale analysis of fire regimes, *Ecosystems*, 10,  
708 809-823, 2007.  
709  
710 Fanin, T., and Werf, G. R.: Precipitation–fire linkages in Indonesia (1997–2015), *Biogeosciences*, 14, 3995-4008,  
711 2017.  
712  
713 Field, R. D., van der Werf, G. R., and Shen, S. S.: Human amplification of drought-induced biomass burning in  
714 Indonesia since 1960, *Nature Geoscience*, 2, 185-188, 2009.  
715  
716 Field, R. D., Van Der Werf, G. R., Fanin, T., Fetzer, E. J., Fuller, R., Jethva, H., Levy, R., Livesey, N. J., Luo,  
717 M., and Torres, O.: Indonesian fire activity and smoke pollution in 2015 show persistent nonlinear sensitivity to  
718 El Niño-induced drought, *Proceedings of the National Academy of Sciences*, 113, 9204-9209, 2016.  
719  
720 Fletcher, K.: SENTINEL 2: ESA's Optical High-Resolution Mission for GMES Operational Services, European  
721 Space Agency, 2012.  
722  
723 Gaveau, D., Salim, M., Hergoualc'h, K., Locatelli, B., Sloan, S., Wooster, M., Marlier, M., Molidena, E., Yaem, H.,  
724 Defries, R., Verchot, L., Murdiyarso, D., Nasi, R., Holmgren, P & Sheil, D.: Major atmospheric emissions from peat  
725 fires in Southeast Asia during non-drought years: evidence from the 2013 Sumatran fires. *Scientific Reports*  
726 4:6112, 2014.  
727  
728 Gaveau, D. L., Pirard, R., Salim, M. A., Tonoto, P., Parks, S. A., and Carmenta, R.: Overlapping land claims limit  
729 the use of satellites to monitor No-Deforestation commitments and No-Burning compliance, *Conservation Letters*,  
730 2017.  
731  
732 [Gaveau, D. L., Santos, L., Locatelli, B., Salim, M. A., Husnayaen, H., Meijaard, E., Heatubun, C., and Sheil, D.:  
733 Forest loss in Indonesian New Guinea \(2001–2019\): Trends, drivers and outlook, \*Biological Conservation\*, 261,  
734 109225, 2021.](#)  
735  
736  
737 Giglio, L., Boschetti, L., Roy, D. P., Humber, M. L., and Justice, C. O.: The Collection 6 MODIS burned area  
738 mapping algorithm and product, *Remote sensing of environment*, 217, 72-85, 2018.  
739  
740 Gorelick, N., Hancher, M., Dixon, M., Ilyushchenko, S., Thau, D., and Moore, R.: Google Earth Engine:  
741 Planetary-scale geospatial analysis for everyone, *Remote Sensing of Environment*, 202, 18-27, 2017.  
742  
743 [Harrison, M. E., Ripoll Capilla, B., Thornton, S. A., Cattau, M. E., and Page, S. E.: Impacts of the 2015 fire season  
744 on peat-swamp forest biodiversity in Indonesian Borneo, \*Peatlands in harmony–Agriculture, industry & nature.\*  
745 \*Proceedings of the 15th international peat congress: Oral presentations, 2016, 713-717.\*](#)  
746  
747 [Hawbaker, T.J., Vanderhoof, M.K., Beal, Y.-J., Takacs, J.D., Schmidt, G.L., Falgout, J.T., Williams, B., Fairaux,  
748 N.M., Caldwell, M.K., Picotte, J.J., Howard, S.M., Stitt, S., Dwyer, J.L., 2017b. Mapping burned areas using  
749 dense time-series of Landsat data. \*Remote Sensing of Environment\* 198, 504–522.](#)  
750  
751  
752 Huang, H., Roy, D. P., Boschetti, L., Zhang, H. K., Yan, L., Kumar, S. S., Gomez-Dans, J., and Li, J.: Separability  
753 analysis of Sentinel-2A Multi-Spectral Instrument (MSI) data for burned area discrimination, *Remote Sensing*, 8,  
754 873, 2016.  
755

756 Huijnen, V., Wooster, M., Kaiser, J., Gaveau, D., Flemming, J., Parrington, M., Inness, A., Murdiyarsa, D., Main,  
757 B., and Van Weele, M.: Fire carbon emissions over maritime southeast Asia in 2015 largest since 1997, Scientific  
758 reports, 6, 26886, 2016.

759

760 Karsai, I., Schmickl, T., and Kampis, G.: Forest Fires: Fire Management and the Power Law, in: Resilience and  
761 Stability of Ecological and Social Systems, Springer, 63-77, 2020.

762

763 ~~Key, C. H., and Benson, N. C.: The Normalized Burn Ratio (NBR): A Landsat TM radiometric measure of burn  
764 severity, United States Geological Survey, Northern Rocky Mountain Science Center.(Bozeman, MT), 1999.~~

765

766 ~~Koplitz, S., Mickley, L., Jacob, D., Marlier, M. E., DeFries, R., Gaveau, D. L., Locatelli, B., Reid, J., Xian, P.,  
767 and Myers, S.: Role of the Madden Julian Oscillation in the Transport of Smoke From Sumatra to the Malay  
768 Peninsula During Severe Non-El Niño Haze Events, Journal of Geophysical Research: Atmospheres, 123, 6282-  
769 6294, 2018.~~

770

771 Koplitz, S. N., Mickley, L. J., Marlier, M. E., Buonocore, J. J., Kim, P. S., Liu, T., Sulprizio, M. P., DeFries, R.  
772 S., Jacob, D. J., and Schwartz, J.: Public health impacts of the severe haze in Equatorial Asia in September-  
773 October 2015: demonstration of a new framework for informing fire management strategies to reduce downwind  
774 smoke exposure, Environmental Research Letters, 11, 094023, 2016.

775

776 ~~Kurniadi, A., Weller, E., Min, S. K., and Seong, M. G.: Independent ENSO and IOD impacts on rainfall extremes  
777 over Indonesia, International Journal of Climatology, n/a, <https://doi.org/10.1002/joc.7040>, 2021.~~

778

779 Liu, S., Zheng, Y., Dalponte, M., and Tong, X.: A novel fire index-based burned area change detection approach  
780 using Landsat-8 OLI data, European journal of remote sensing, 53, 104-112, 2020.

781

782 ~~Lizundia-Loiola, J., Otón, G., Ramo, R., and Chuvieco, E.: A spatio-temporal active-fire clustering approach for  
783 global burned area mapping at 250 m from MODIS data, Remote Sensing of Environment, 236, 111493, 2020.~~

784 ~~Lizundia-Loiola, J., Franquesa, M., Boettcher, M., Kirches, G., Pettinari, M. L., and Chuvieco, E.: Operational  
785 implementation of the burned area component of the Copernicus Climate Change Service: from MODIS 250 m  
786 to OLCI 300 m data, Earth System Science Data Discussions, 1-37, 2021.~~

787

788

789 Lohberger, S., Stängel, M., Atwood, E. C., and Siegert, F.: Spatial evaluation of Indonesia's 2015 fire-affected  
790 area and estimated carbon emissions using Sentinel-1, Global change biology, 24, 644-654, 2018.

791

792 Malamud, B. D., Morein, G., and Turcotte, D. L.: Forest fires: an example of self-organized critical behavior,  
793 Science, 281, 1840-1842, 1998.

794

795 ~~Marlier, M. E., DeFries, R. S., Voulgarakis, A., Kinney, P. L., Randerson, J. T., Shindell, D. T., Chen, Y., and  
796 Faluvegi, G.: El Niño and health risks from landscape fire emissions in southeast Asia, Nature climate change, 3,  
797 131-136, 2013.~~

798

799

800 ~~Miettinen, J., Shi, C., and Liew, S.-C.: Fire distribution in Peninsular Malaysia, Sumatra and Borneo in 2015 with  
801 special emphasis on peatland fires, Environmental management, 60, 747-757, 2017.~~

802

803 ~~Nikonovas, T., Spessa, A., Doerr, S. H., Clay, G. D., and Mezbahuddin, S.: Near complete loss of fire-resistant  
804 primary tropical forest cover in Sumatra and Kalimantan, Communications Earth & Environment, 1, 1-8, 2020.~~

805

806 Olofsson, P., Foody, G. M., Herold, M., Stehman, S. V., Woodcock, C. E., and Wulder, M. A.: Good practices  
807 for estimating area and assessing accuracy of land change, Remote Sensing of Environment, 148, 42-57,  
808 <http://dx.doi.org/10.1016/j.rse.2014.02.015>, 2014.

809

810 ~~Otón, G., Ramo, R., Lizundia-Loiola, J., and Chuvieco, E.: Global detection of long-term (1982-2017) burned  
811 area with AVHRR-LTDR data, Remote Sensing, 11, 2079, 2019.~~

812

813

814 ~~Ramo, R., Roteta, E., Bistinas, I., Van Wees, D., Bastarrika, A., Chuvieco, E., and Van der Werf, G. R.: African  
815 burned area and fire carbon emissions are strongly impacted by small fires undetected by coarse resolution satellite  
816 data, Proceedings of the National Academy of Sciences, 118, 2021.~~

817  
818 Ritung, S., Wahyunto, Nugroho, K., Sukarman, Hikmatullah, Suparto, and C, T.: Peatland map of Indonesia,  
819 Department of Research and Development of Agricultural Land Resources, Ministry of Agriculture, 2011.  
820  
821 Rochmyaningsih, D.: Wildfire researcher deported amid growing rift between Indonesian government and  
822 scientists, *Science*, 367, 722-723, 2020.  
823  
824 [Sipongi.](http://sipongi.menlhk.go.id/hotspot/luas_kebakaran) Recapitulation of Land and Forest Fires Area (Ha) per Province in Indonesia 2015-2020:  
825 [http://sipongi.menlhk.go.id/hotspot/luas kebakaran](http://sipongi.menlhk.go.id/hotspot/luas_kebakaran), 2020.  
826  
827 Sloan, S., Locatelli, B., Wooster, M. J., and Gaveau, D. L.: Fire activity in Borneo driven by industrial land  
828 conversion and drought during El Niño periods, 1982–2010, *Global environmental change*, 47, 95-109, 2017.  
829  
830 Sloan, S., Tacconi, L., and Cattau, M.: Fire prevention in managed landscapes: ~~Successes and limitations~~Recent  
831 success and challenges in Indonesia, *Mitigation and Adaptation Strategies for Global Change*, 26: Article 32,  
832 2021 Under Review.  
833  
834 Stehman, S. V., Wickham, J., Smith, J., and Yang, L.: Thematic accuracy of the 1992 National Land-Cover Data  
835 for the eastern United States: Statistical methodology and regional results, *Remote Sensing of Environment*, 86,  
836 500-516, 2003.  
837  
838 Tansey, K., Beston, J., Hoscilo, A., Page, S., and Paredes Hernández, C.: Relationship between MODIS fire hot  
839 spot count and burned area in a degraded tropical peat swamp forest in Central Kalimantan, Indonesia, *Journal of*  
840 *Geophysical Research: Atmospheres*, 113, 2008.  
841  
842 [Van der Werf, G. R., Dempewolf, J., Trigg, S. N., Randerson, J. T., Kasibhatla, P. S., Giglio, L., Murdiyarso, D.,](#)  
843 [Peters, W., Morton, D., and Collatz, G.: Climate regulation of fire emissions and deforestation in equatorial Asia,](#)  
844 [Proceedings of the National Academy of Sciences, 105, 20350-20355, 2008.](#)  
845  
846  
847 [Van Der Werf, G. R., Randerson, J. T., Giglio, L., Van Leeuwen, T. T., Chen, Y., Rogers, B. M., Mu, M., Van](#)  
848 [Marle, M. J., Morton, D. C., and Collatz, G. J.: Global fire emissions estimates during 1997–2016, \*Earth System\*](#)  
849 [Science Data, 9, 697-720, 2017.](#)  
850  
851  
852 van Nieuwstadt, M. G. L., and Sheil, D.: Drought, fire and tree survival in a Borneo rain forest, East Kalimantan,  
853 Indonesia, *Journal of Ecology*, 93, 191-201, 2005.  
854  
855 [Watts, J. D., Tacconi, L., Hapsari, N., Irawan, S., Sloan, S., and Widiastomo, T.: Incentivizing compliance:](#)  
856 [Evaluating the effectiveness of targeted village incentives for reducing burning in Indonesia, \*Forest Policy and\*](#)  
857 [Economics, 108, 101956, 2019.](#)  
858  
859 Wooster, M., Gaveau, D., Salim, M., Zhang, T., Xu, W., Green, D., Huijnen, V., Murdiyarso, D., Gunawan, D.,  
860 and Borchard, N.: New tropical peatland gas and particulate emissions factors indicate 2015 Indonesian fires  
861 released far more particulate matter (but less methane) than current inventories imply, *Remote Sensing*, 10, 495,  
862 2018.  
863  
864  
865  
866  
867  
868  
869

870

871

872

873

874

875

876

877

878

879

880

881

882

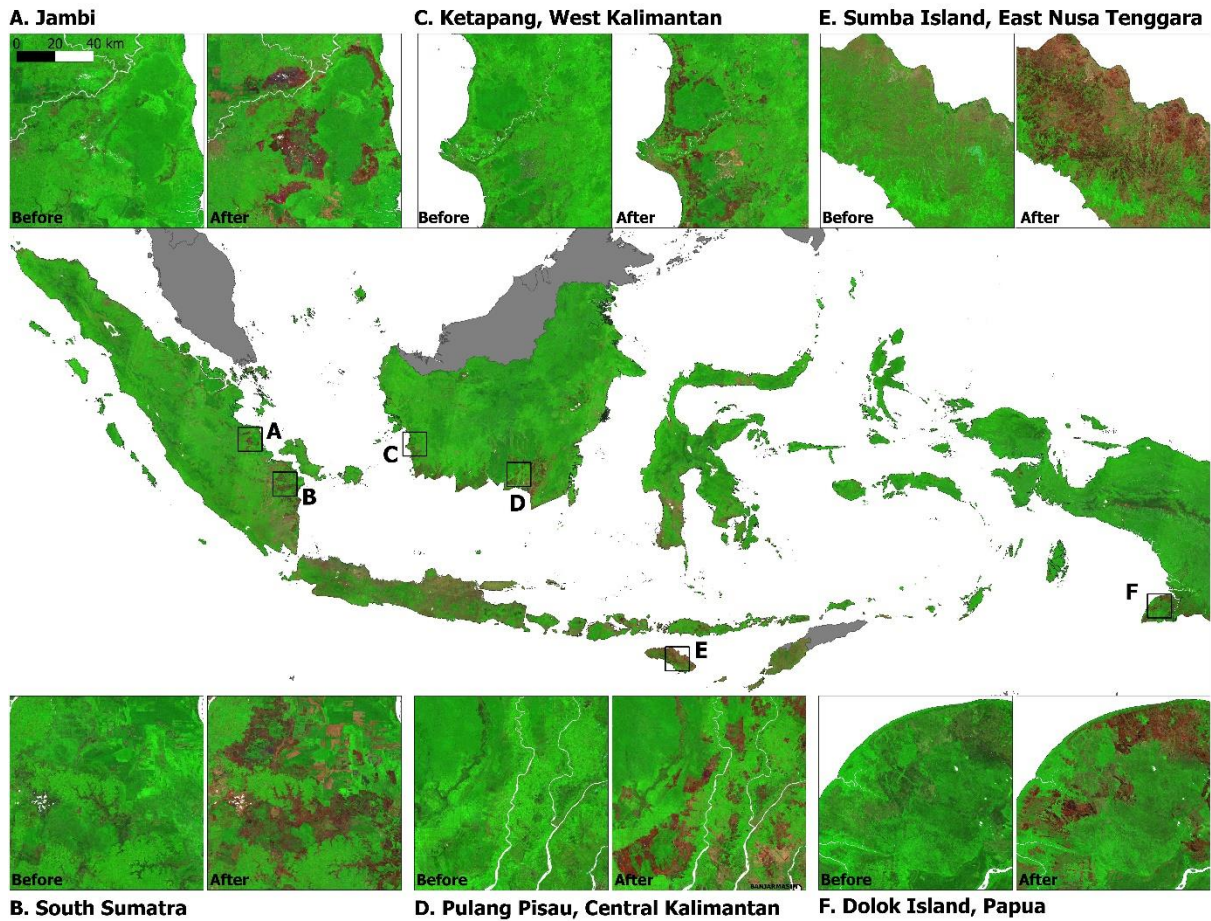
883

884

885 **Figures**

886

887



888

**B. South Sumatra**

**D. Pulang Pisau, Central Kalimantan**

**F. Dolok Island, Papua**

889

**Figure 1.** The pair of cloud-free pre-and post-fire Sentinel-2 composites shown over six locations in insets A, B, C, D, E, F (all insets have the same scale). The base Indonesia-wide imagery is the post-fire composite. Imagery displayed in false colors (RGB: short-wave infrared (band 11); Near infrared (band 8), Blue: red (band 4)). In this pair of composite images acquired shortly before and after fire a recently burned area will readily appear to have transitioned from 'green' to dark 'brown/red' tones. Areas cleared without burning appear bright pink. Areas covered with vegetation appear dark to bright green.

894

895

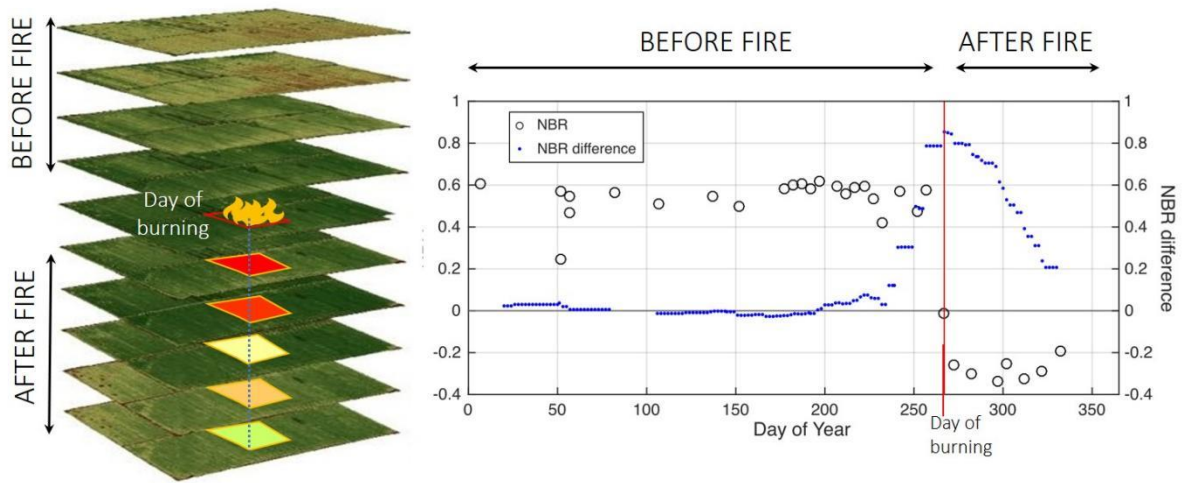
896

897

898

899

900

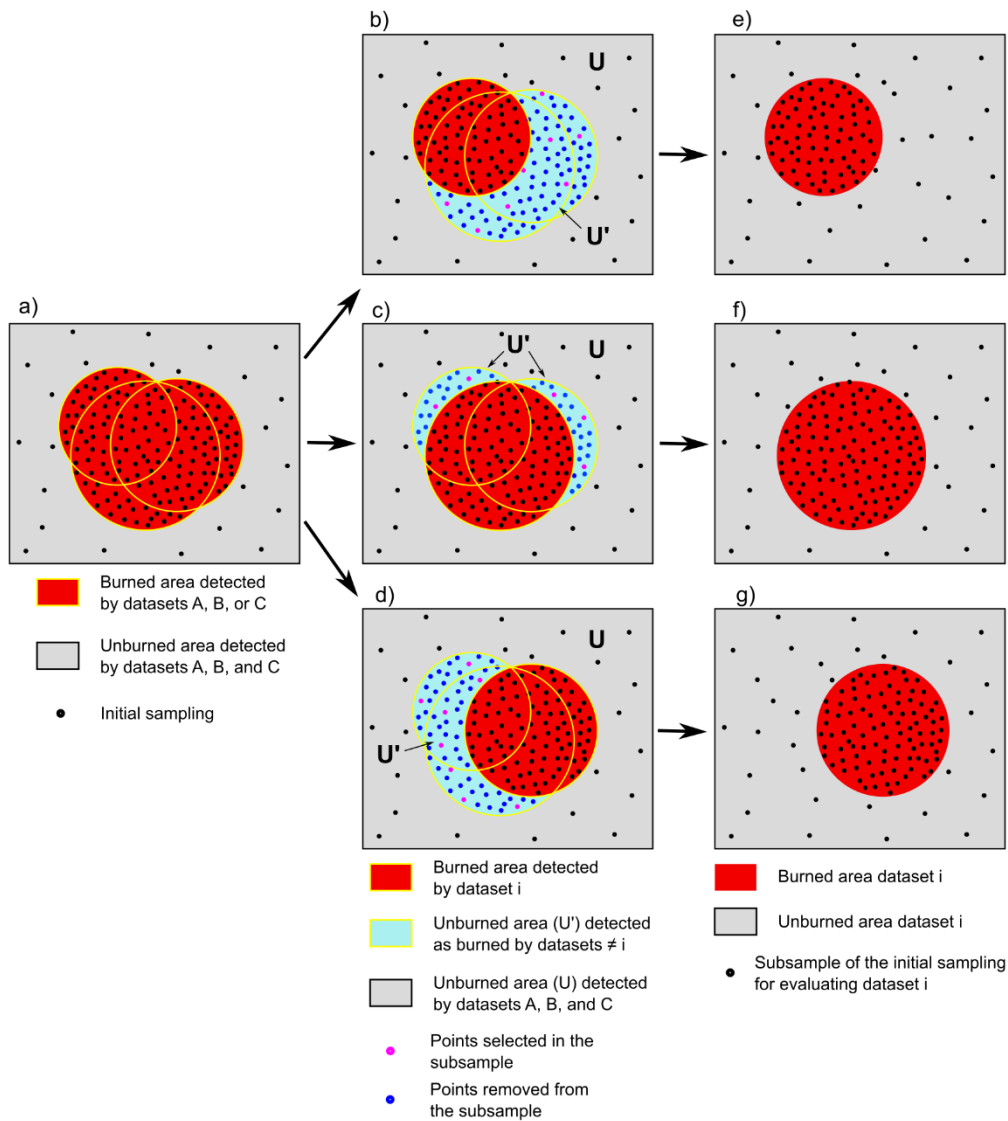


901

902 **Figure 2.** A schematic of Sentinel-2 time-series imagery, associated NBR values (open circles) and NBR differences between  
 903 average NBR values observed before and after the central day of a 2-day moving window (blue dots). A burned pixel (20 m x  
 904 20 m) is represented by a red rectangle at left. Before fire, the vegetated pixel registers positive NBR values (open circles).  
 905 The NBR rapidly drops during the fire and, for a few weeks, the satellite observations show a negative NBR. The day of the  
 906 year when the NBR difference observed via the moving window reaches a maximum corresponds to the moment NBR dropped  
 907 (red line). This day marks a decline in the pixel's vegetation, possibly reflecting a burning event. Over time, the vegetation  
 908 regenerates (re-greening) and the spectral characteristic of charred vegetation fades. Regreening can happen within days in the  
 909 case of savanna grasslands, or within months in the case of forest fires on peatlands.

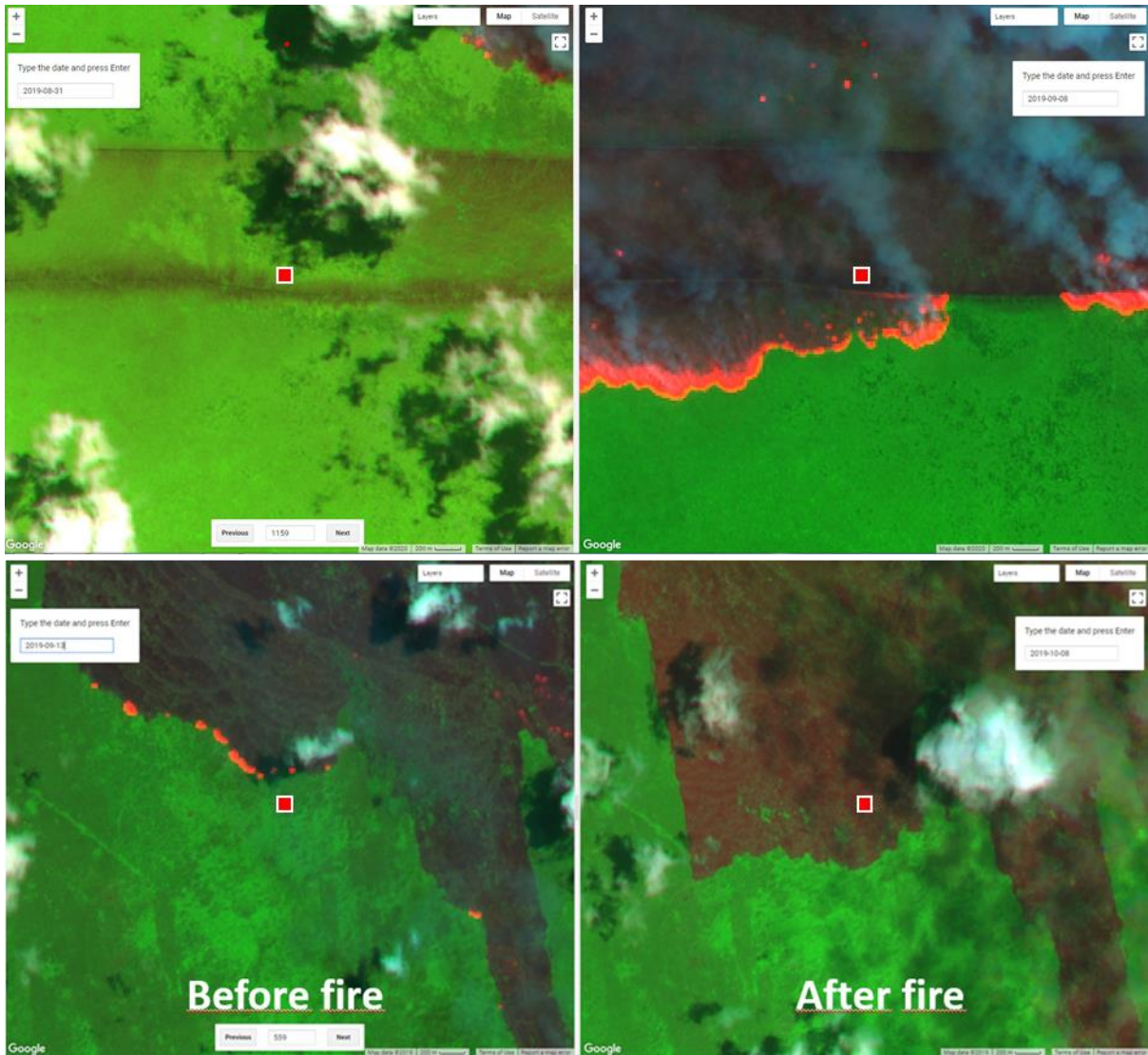
910  
 911  
 912  
 913





914

915 **Figure 3.** Representation of the adjusted, stratified-sampling design for the validation of three burned area datasets (A, B, and  
 916 C) against reference sites (dots). Panel (a) shows the stratified random sampling of reference sites (black points) over the  
 917 combined burned area. Note that the density of samples is higher in the combined burned area than the unburned area. Panels  
 918 (b), (c), and (d) show, in cyan, the area  $U'$ , being classified as unburned in a given dataset  $i$  but classified as burned in at least  
 919 one other datasets  $\neq i$ . For a given validation of A, B, and C, the sample points in the corresponding area  $U'$  (panels (b), (c),  
 920 (d)) were randomly excluded until the sampling density in the area  $U'$  equaled that of the larger unburned area  $U$  (area in  
 921 gray). Panels (e), (f) and (g) show the three final, adjusted, stratified subsamples of reference points derived from the  
 922 initial sample of 1298 reference points. Note that the relative areas and number of sites per class in Figure 3 do not correspond  
 923 to the actual datasets being evaluated.



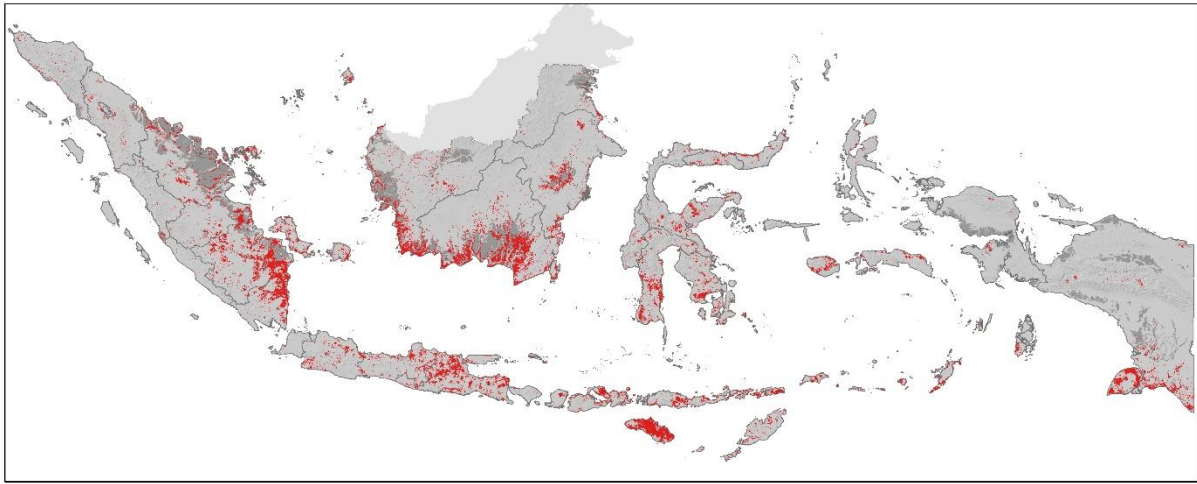
924

925 **Figure 4.** Two snapshots recording the pre-fire (left panel) and post-fire (right panel) original Sentinel-2 images acquired  
 926 shortly before (13 September 2019) and shortly after (08 October 2019) fire for two reference site (red squares). Imagery  
 927 displayed in RGB: SWIR, NIR, RED. Sentinel-2 provides two SWIR Bands. Band 12=2.190  $\mu\text{m}$  is more suitable than Band  
 928 11=1.610  $\mu\text{m}$  to detect the intense heat from flaming fronts. On these image pairs, one can see flaming fronts traveling towards  
 929 the reference sites (red dot) from the north on the pre fire images (left), and sharp changes in color from 'green' to 'dark red'  
 930 characteristic of charred remains with continuing flaming on the post-fire images (right). Layout built using © Google Earth  
 931 Engine.

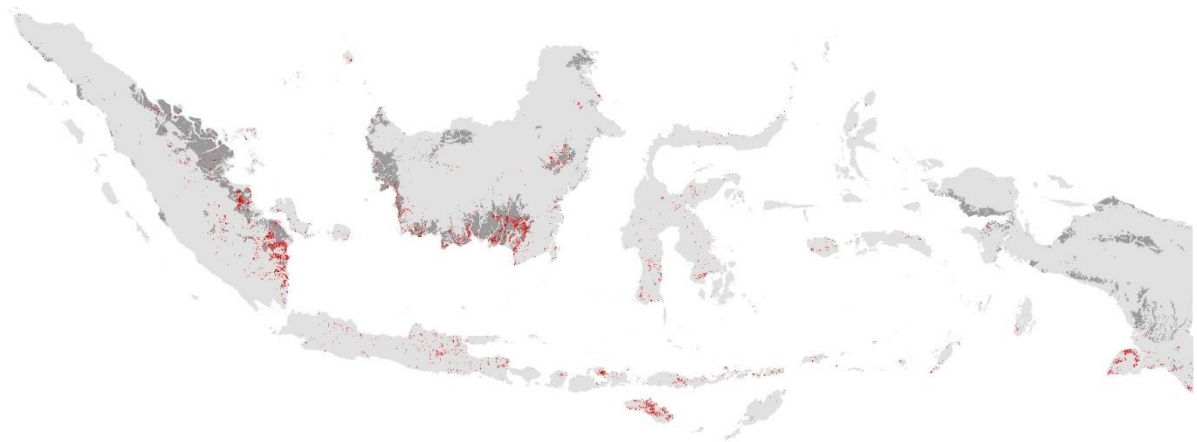
932

933

934

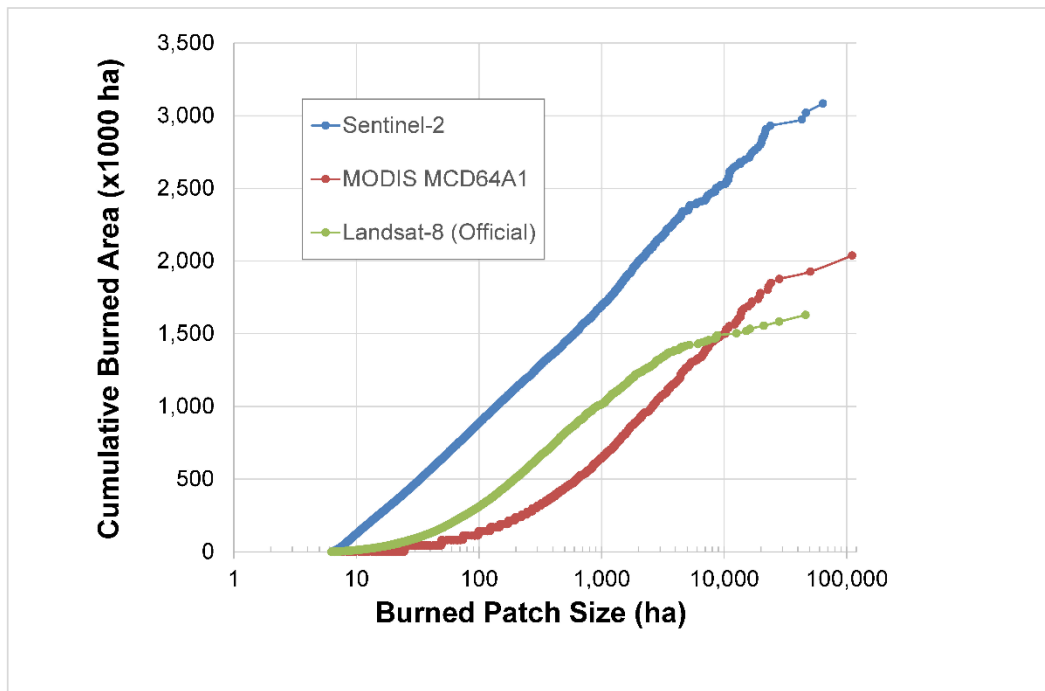


935

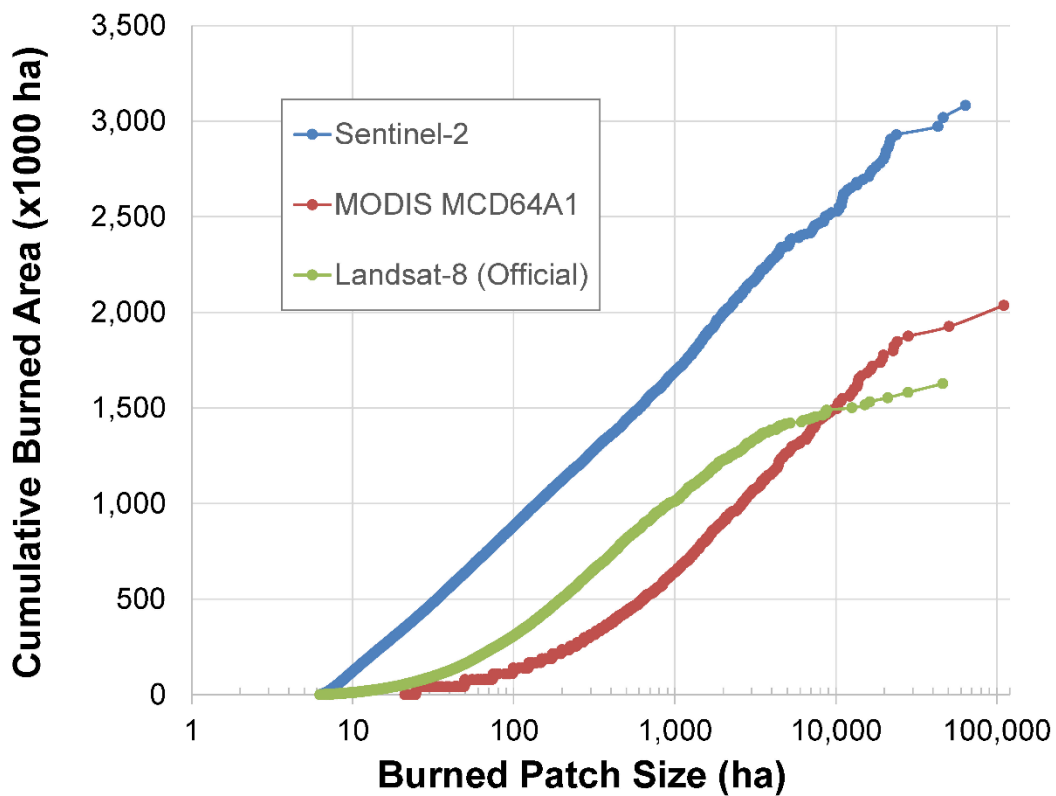


936

937 **Figure 5.** 2019 burned areas (red) for Indonesia (grey area) derived using a time-series of the atmospherically corrected surface  
 938 reflectance multispectral images (level 2A product) taken by the Sentinel-2 A and B satellites. The spatial resolution of this  
 939 map is 20 m x 20 m, and mMinimum mapping unit is 6.25 ha. The officially recognized peatlands extent is shown with the  
 940 darkest shade of grey. A provincial breakdown of burned areas according to our map estimates and those of the Official and  
 941 the MCD64A1 product are given in Figure S54.  
 942



943

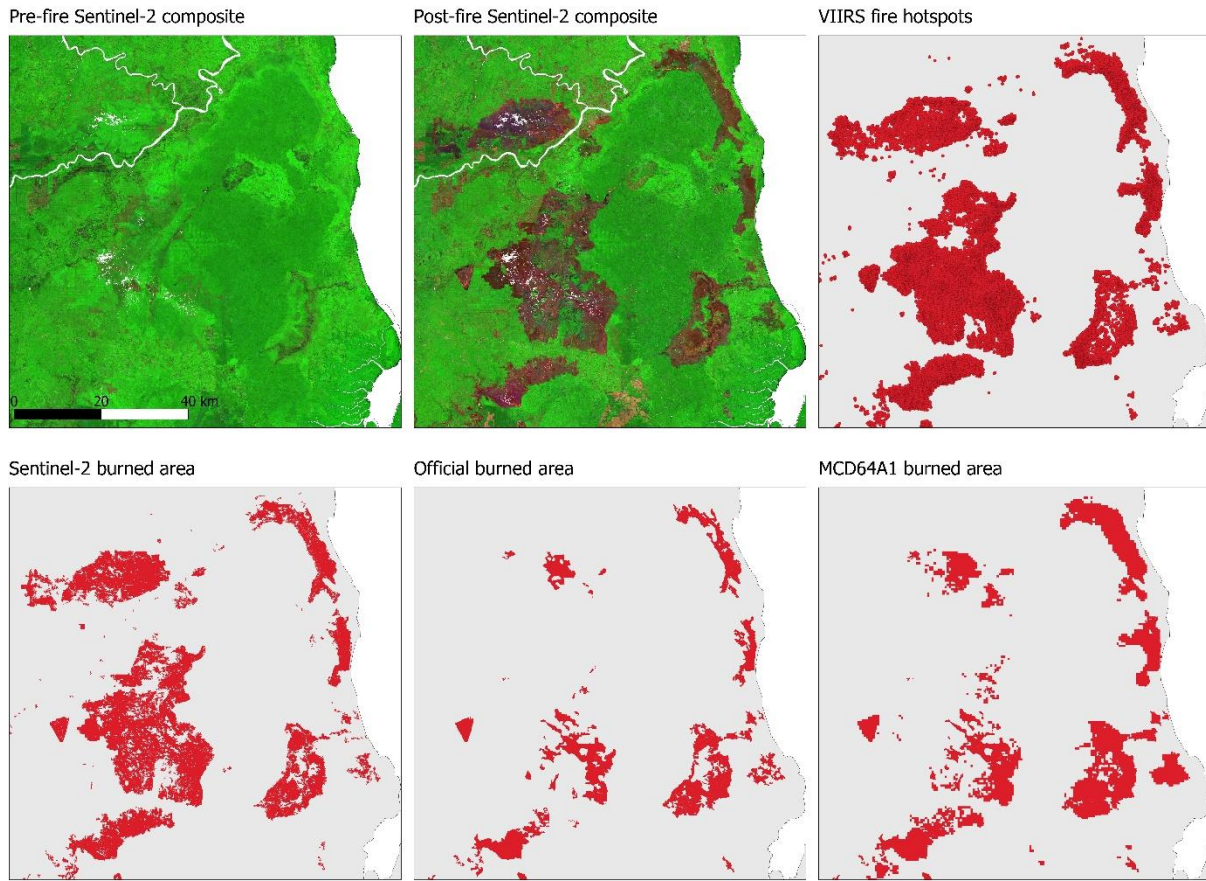


944

945 **Figure 6.** Cumulative national total burned area versus burned-scar area, for Sentinel-2, Landsat-8 (Official), and MODIS  
 946 MCD64A1 burned-area estimates. ~~Scars < 6.25 ha are not shown.~~ Note the logarithmic axis. For a given segment of the x-  
 947 axis between scar sizes  $X_1$  and  $X_2$ , a difference in the slopes for any two estimates is indicative of inter-estimate differences  
 948 in terms of inclusivity of scars between  $X_1$  and  $X_2$ .  
 949

950

951



952

953 **Figure 7.** The pair of cloud-free pre-and post-fire Sentinel-2 composites over Berbak National Park (black line) and  
 954 surrounding areas in Jambi Province (see also Inset A, Figure 1), revealing large, burned areas around Berbak National Park  
 955 (areas that have transitioned from ‘green’ to dark ‘brown/red’ tones). These large burn scars have been detected by VIIRS  
 956 hotspots and by the Sentinel-2 burned area map, but some have been missed by the Official and MCD64A1 datasets.  
 957

958

959

960

961

962

963

964

965

966

967

968

969

970

971 **Tables**

972

973 **Table 1.** Adjusted, Stratified Subsamples of Reference Sites to Validate Burned-Area Estimates.

Burned-Area Estimate	Reference Sites		Total Reference Sites
	In Areas Classified as Burned	In Areas Classified as Unburned (U & U')	
Sentinel-2 (this study)	888	280	1168
MODIS MCD64A1	891	242	1133
Landsat-8 (Official)	895	182	1077

974

975 **Table 2.** Accuracy assessment of each of the three burned area maps performed in seven Indonesian provinces (87.60 Mha)  
 976 targeted for peatland restoration. The accuracy metrics were estimated with an initial total of 1,298 points randomly distributed  
 977 using stratified sampling. The reported metrics are: 1) the overall accuracy (OA), the user's accuracy (UA), and the producer's  
 978 accuracy (PA) with their 95% confidence intervals, and 2) the mapped burned area and the corrected burned area with their  
 979 95% confidence intervals.

	SENTINEL	OFFICIAL	MCD64A1
OA (%)	99.3 (99.1, 99.6)	98.1 (97.8, 98.5)	98.4 (98.1, 98.8)
UA (%)			
Burned	97.9 (97.1, 98.8)	95.1 (93.5, 96.7)	76.0 (73.3, 78.7)
Unburned	99.3 (99.1, 99.6)	98.6 (98.2, 99.0)	98.8 (98.5, 99.2)
PA (%)			
Burned	75.6 (68.3, 83.0)	49.5 (42.5, 56.6)	53.1 (45.8, 60.5)
Unburned	99.9 (99.9, 99.9)	99.9 (99.9, 99.9)	99.6 (99.6, 99.7)
Mapped burned area (Mha)	1.84	1.19	1.58
Corrected burned area (Mha)	2.38 (2.14, 2.61)	2.29 (1.96, 2.63)	2.27 (1.94, 2.59)
Difference (Mha)	0.54	1.1	0.69

980

981 **Table 3.** Tests statistics with respect to three-way differences in burned area scar-size frequency distributions for Sentinel,  
 982 MODIS, and official estimates.

Scar Size (ha)	Kruskal-Wallis H <sup>a</sup>
> <del>6.25</del>	10,478**
> <del>20-25</del>	998*
> 100	335*
> 1000	14*
> 5000 <sup>a</sup>	0.61

983

984 Significance: \*\* p&lt;0.0001; \* p&lt;0.001

985 Notes: Scar-size thresholds in the table denote the set of scars included in a test. Tests pertain to whether frequency  
 986 distributions have equivalent 'distribution location', that is, position along a continuum of scar sizes. Tests thus pertain to  
 987 whether the estimates capture distinct realms of fire activity, assuming similarly shaped frequency distributions. Higher test  
 988 statistic values indicate greater probability that the estimates differ with respect to distribution location. The tree-way  
 989 comparisons of the estimates may flag differences where all three estimates differ or where only two of the three differ.  
 990 Significance is not Bonferroni corrected. (a) There are 56, 60 and 16 scars > 5000 ha for Sentinel, MCD64A1, Official  
 991 estimates, respectively.

992

993

994

996 **Table 4.** Test statistics with respect to two-way differences in burned area scar-size frequency distributions, with respect to  
 997 distribution shape and situation (Test I) or situation alone (Test II), for Sentinel estimates compared to either MCD64A1 or  
 998 Official estimates.  
 999

Scar Size (ha)	Sentinel vs. MCD64A1		Sentinel vs. Official			
	<i>I. Kolmogorov-Smirnov (Most Extreme Difference [positive/negative])<sup>b</sup></i>	<i>Z-score</i>	<i>II. Mann-Whitney U Z-score</i>	<i>I. Kolmogorov-Smirnov (Most Extreme Difference [positive/negative])<sup>b</sup></i>	<i>Z-score</i>	<i>II. Mann-Whitney U Z-score</i>
> 6.25	N/A	46.9** (+0.69)	-82.9**	31.8** (+0.32)		-70.6**
> 250		14.7** (+0.24/-0.15)	-20.1*	13.2** (+0.18)		-28.6*
> 100		7.9** (+0.23)	-16.6*	1.6 <sup>†</sup> (+0.04/-0.04)		-0.57
> 1000		0.76 (+0.06/-0.03)	-0.79	1.5 <sup>‡</sup> (+0.01/-0.12)		-3.1*
> 5000 <sup>a</sup>		0.72 (+0.14/-0.08)	-0.77	0.70 (+0.13/-0.20)		0.10

1000  
 1001  
 1002  
 1003  
 1004  
 1005  
 1006  
 1007  
 1008  
 1009  
 1010  
 1011

Significance: \*\* p<0.0001; \* p<0.001; • p<0.01; † p=0.014; ‡ p<0.05  
 Notes: Scar-size thresholds denote the cohort of scars included in a test. Test I and Test II both pertain to whether the Sentinel estimates capture distinct realms (scar-size cohorts) of fire activity compared to the other two estimates. Test I pertains to whether the scar-size frequency distribution of the Sentinel estimate has the same shape and 'distribution location' as either the MODIS or official estimate. Test II is the same but with respect to distribution location only. Distribution location refers to the situation of a frequency distribution along a continuum of scar sizes. Higher test statistics indicate greater probability that the estimates differ significantly with respect to distribution shape and/or location. Reported statistical significance is without Bonferroni corrections. a) There are 56, 60 and 16 scars > 5000 ha for Sentinel, MODIS, official estimates, respectively. (b) Largest positive and negative differences in the cumulative probability functions of Sentinel vs. MODIS or official scar-size estimates. No difference was reported where it was <0.00 absolutely.